Proximity Effects in Electronic Metal-Support Interactions: O-Vacancy Formation and CO adsorption on Ru/ZrO_2 Model Catalysts

Mengru Li, Axel Groß and R. Jürgen Behm

Institute of Theoretical Chemistry, Ulm University, Oberberghof 7, D-89081 Ulm, Germany

Abstract

ABSTRACT: Continuing our investigation of electronic metal−support interactions (EMSIs) in heterogeneous catalysis, we have investigated the influence of the position and the number of O-vacancies on their stabilization by the Ru nanorod, on the charge transfer from the support to the metal, and on CO adsorption on the Ru nanorod. Employing density functional theory based calculations and using a model system consisting of a ZrO_2(111) support and a three-layer Ru nanorod, we find that O-vacancies are significantly stabilized only if they are in direct contact to the Ru nanorod, with the extent of stabilization depending on the distance between vacancy and the nearest Ru atom at the interface. Vacancy formation aside the Ru nanorod or in deeper layers of the support is not enhanced by the metal. The Ru induced stabilization of the O-vacancies is closely coupled with the charge transfer from the support to the metal upon vacancy formation, which is true also in the presence of neighbored O-vacancies.

The CO adsorption energy can be substantially modified by four characteristic effects, including charge transfer from the support to the metal, coordination effects, a combination of CO_{ad} induced deformation energies and changes in the interface energy and direct interactions between CO and partly reduced Zr surface ions directly neighbored to an O-vacancy, depending on the adsorption site and on the number and positions of the O-vacancies. Thus, it is not possible to completely describe the adsorption properties by using the d-band model, in particular not for adsorption on the interface sites. The general relevance of this findings for adsorption and catalytic reactions is discussed.

Keywords: *Catalysis, adsorption, vacancy formation, electronic metal-support interactions, DFT calculations, Ru, ZrO_2, CO*

1 Introduction

Supported metal catalysts, consisting of metal nanoparticles of a few nm in diameter supported on high-surface-area materials, mostly oxides, play a key role in heterogeneous catalysis.[1-3] While initially, the support was assumed to be catalytically inert and mainly served to stabilize and separate the active metal nanoparticles, this picture changed with time.[4] Already in the late 1970s, Tauster introduced the concept of 'strong metal - support interactions (SMSIs)', according to which the catalytic activity of the catalyst can be modified (and mainly lowered) by partial overgrowth of the metal surface by a thin layer of the partly reduced oxide.[5-7] In 2012, Campbell introduced 'electronic metal - support interactions (EMSIs)' as another fundamentally different type of metal - support interactions (MSIs),[8] based on work by Bruix et al.[9] In this case, the adsorption / reaction behavior of the metal surface sites was modified by charge transfer between support and metal NP (for recent overviews see [10-12]). Furthermore, it turned out that in addition to other physical parameters of the catalyst such as the size of the metal nanoparticles, the chemical potential of the metal atoms in these particles, [13;14] or their oxophilicity,[13] also the reducibility of the support plays an important if not decisive role.[15] It allows to tune the charge transfer to the metal nanoparticle and thus their reactivity via formation of O-vacancies [16-19] or even oxidation reactions to proceed via a Mars – van Krevelen reaction mechanism.[18;19] Details of the charge transfer process and its impact on the adsorption and reaction characteristics as well as of their range, however, are still under debate. These aspects are topic of the present study, where we investigated O-vacancy formation and their impact on the CO adsorption characteristics on $Ru/ZrO_2(111)$ model catalysts. .

Recently, we had investigated the CO_2 methanation reaction on a Ru/ZrO_2 catalyst in a combined experimental and theoretical approach, including also extensive density functional theory (DFT) based calculations on a $Ru/ZrO_2(111)$ model catalyst system.[20;21] In that work we had demonstrated that the formation of surface O-vacancies can by enhanced and stabilized by

the presence of metal nanoparticles (NPs), in this case of a Ru nanorod: The formation of a surface O-vacancy at the interface, i.e., directly underneath the Ru nanorod, was found to lead to a significant transfer of (negative) charge to neighboring Ru atom(s) at the interface and furthermore also to an increase of the CO adsorption energy on these sites. In contrast, metal atoms further apart from the O-vacancy and the interface, e.g., in the second or third layer of the three-layer Ru nanorod, were little affected by these O-vacancies.[21] These results indicated that charge transfer from the O-vacancy to the metal is essentially limited to the metal atoms directly at the metal-oxide interface. This is in contrast to the commonly published statement of a charge transfer to the (entire) metal nanoparticle,[22] which was concluded, e.g., from shifts of the vibrational features of the adsorbed species detected experimentally.[23;24] This has considerable consequences on the fundamental understanding of the role of O-vacancies in catalytic reactions on metal catalysts supported on reducible oxides, as only a small fraction of the accessible metal surface atoms will be modified, namely those at the interface perimeter of the metal nanoparticles. The other ones, which depending on the shape and size of the NPs may often represent the majority of surface atoms, maintain their typical character as essentially charge-neutral metal atoms. Considering the close correlation between local adsorption strength and catalytic activity, which is well known as the Sabatier principle,[25] these interface perimeter sites may thus represent (more) active sites in a catalytic reaction. Thus, the introduction of vacancies allows to tune the reactivity of the metal surface sites at the interface.[26]

While these general principles had been clarified in the previous calculations,[21] supported also by experimental findings,[20] several important aspects are still open. These include first the question whether the limitation to a strictly local effect is true also for O-vacancy formation, or whether O-vacancies closely aside or deeper underneath the metal nanorod can also be stabilized by the metal nanoparticle/nanorod (see Figure 1a and 1b, c). One could imagine that the formation of several O-vacancies (vacancy clusters), either aside the Ru nanorod in the

topmost layer or reaching from the metal-oxide interface to deeper layers, could result in an enhanced charge transfer from the more remote O-vacancy. These points are essential for clarifying whether the formation of O-vacancies slightly off from the metal-oxide interface is energetically favorable as well, or whether in these cases the energetics are rather similar to O-vacancy formation in the absence of metal NPs. A second important question deals with the effect of O-vacancies on the CO adsorption behavior, in particular on the CO adsorption energy and the vibrational properties. The CO adsorption energy is not only highly relevant, e.g., for all catalytic reactions where it serves as descriptor for the activity of the respective catalyst. Moreover, based on the scaling relations, the CO adsorption energy can also be considered as an indicator for the adsorption strength of other chemisorbed species. Thus, the possibility of tuning the CO adsorption energy and its comprehensive understanding are highly relevant also for applications.

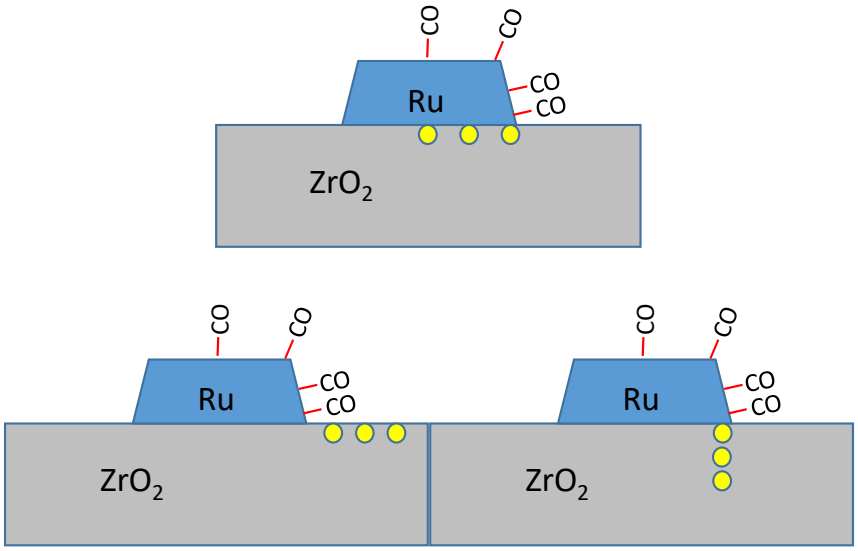

Figure 1: Schematic representation of the O-vacancy formation in direct contact (a) and in close proximity, but not in direct contact to the metal nanoparticle (b, c), and the effect on CO adsorbed on different metal sites.

These aspects are addressed in the present work. Building on the previous calculations and experiments we explore the effect of moving an O-vacancy laterally underneath the metal-oxide

interface or slightly away from the interface, either laterally or vertically, on the vacancy formation energy (section 3.1), on the charge transfer to the Ru nanorod and to the different Ru adsorption sites as well as on the CO adsorption energy (sections 3.2.1 – 3.2.3). Section 3.2 also contains a brief evaluation and discussion of the influence of adsorbed CO on the O-vacancy formation energy (section 3.2.4). In both parts, sections 3.1 and 3.2, we are particularly interested in deriving general principles and correlations such as the empirically established correlation between the position of the center of the d-band on the adsorption site and the adsorption energy on this site, as well as in deviations from these correlations that seem to be specific for supported metal nanostructures as compared to smooth metal surfaces. Focusing on CO adsorption, these are discussed in section 3.2.5. Finally, we will test whether the trends in adsorption energy fit to the trends in the calculated vibrational properties of the adsorbed CO (C-O stretch frequency) (section 3.3).

2 Computational Details

The computational setup is very similar to the one described previously.[20;21] In short, spin-polarized periodic DFT calculations were performed utilizing the Vienna ab initio software package (VASP),[27-29] with ionic cores described by the projected augmented wave (PAW) method.[30;31] The Perdew-Burke-Ernzerhof (PBE) functional [32] was used for exchange-correlation energies within the generalized gradient approximation (GGA). The cut-off energy of the plane wave basis in the expansion of the wave functions was set to be 600 eV. On-site Coulomb interactions were considered using the DFT+U approach [33;34] to treat the highly localized 4d states of Zr. The parameter U-J = 4.00 eV was taken from a previous work.[35] Dispersion corrections were included within the DFT-D3 method.[36] The k-point mesh was set to be 3 × 3 × 1 for the slab calculations, due to the negligible energy variation obtained for 5 × 5 × 1 and 3 × 3 × 1 meshes for the (1 × 3) super cell of ZrO_2(111). A k-point mesh of 9 × 9 × 9

[37] was utilized to optimize the bulk structure of the ZrO_2 support. Here we used the monoclinic γ-phase, which is the most stable phase at room temperature. Ionic bulk relaxations were considered to reach convergence for forces below 0.001 eV/Å. We employed the charge partitioning method reported by Manz et al. [38;39] to calculate local charges. This method is well-suited for strongly polarized systems.[40] However, we also tested this approach against alternative charge partition schemes, which resulted in consistent trends regarding alterations and disparities in the charge states.

For the description of the Ru/ZrO_2 catalyst we modified the $Ru/ZrO_2(111)$ model described in our previous work by removing the bottom three layers of the support to reduce the computational cost.[20] This adjustment resulted in changes of the O-vacancy formation energy and in the CO adsorption energy of below 0.10 eV. Thus, the overall trends in these properties derived in our previous work remained unaffected, while specific number may change slightly. Overall, the Ru/ZrO_2 model catalyst consists of a three-layer $[11\bar{2}0]$ oriented Ru nanorod with a (3 × 3) super cell of Ru(0001), which is positioned on a five-layer (1 × 3) super cell of $ZrO_2(111)$ (see Figure 2). The bottom two layers of ZrO_2 were fixed, while the Ru atoms and the uppermost three layers of the $ZrO_2(111)$ support were relaxed for optimization. Subsequently, we constructed Ru/ZrO_{2-x} catalysts with varying O-vacancy concentrations and distributions by removing specified lattice oxygen atoms. Systems with individual O-vacancies were modeled by removing one lattice oxygen atom per unit cell. We investigated O-vacancies located in different positions: in the uppermost layer and deeper layers underneath the Ru nanorod, as well as in the top layer of the support adjacent to the Ru nanorod. Among the 15 O atoms in the uppermost layer, labeled as n_i (i=1-15) in Figure 2c, nine (from 1i to 9i) are covered by the Ru nanorod, denoted as 'lattice-O atoms underneath the Ru nanorod'. The remaining six O-atoms, labeled from 10i to 15i, were distributed on both sides of the Ru nanorod without direct contact with the Ru nanorod. Furthermore, O-vacancies underneath the edge of Ru

nanorod in deeper layer, i.e., on ii, iii, or iv sites, were created as depicted in Figure 2b. The distance between these O-vacancies and the nearest Ru atom increases from 3.89 Å to 5.14 Å and 6.29 Å, respectively.

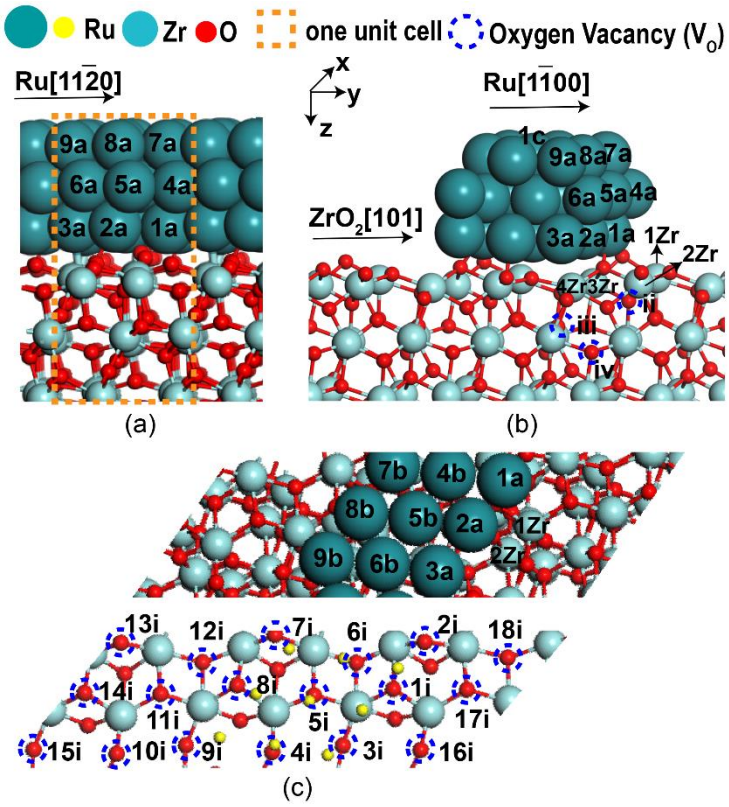

Figure 2. Side-views (a) and (b) and top-view (c) of the Ru/ZrO_2(111) model system, illustrating also the numbering of the different sites. The coordinate system is indicated in Figure 2b, with the x-axis pointing along the Ru nanorod. The notations ni represent individual oxygen vacancy (O_v) positions in the top layer directly underneath or aside the Ru nanorod, ii, iii, and iv denote positions in deeper layers underneath the Ru nanorod. Formation of O-vacancies on positions 1i, 2i, 3i, 4i, and 5i leads to oxygen vacancy (O_v) clusters $1V_O$, $2V_O$, $3V_O$, $4V_O$, and $5V_O$ with 1 – 5 O-vacancies in the top layer underneath the Ru nanorod, as illustrated in the schematic representation in Table 1 in our previous report.[21] O-vacancies on positions 1i, 17i, 18i, and 14i lead to O-vacancy clusters $1V_O$, $2V_O$, $3V_O$, and $4V_O$ in the top layer of the support directly adjacent to the Ru nanorod. Finally, positions ii, iii, and iv refer to newly formed O_v sites in the deeper layers underneath the Ru nanorod, which starting from the O_v at site 1i contribute to the formation of the O_v clusters $1V_O$, $2V_O$, $3V_O$, and $4V_O$.

This also allowed us to separate changes in the vacancy formation energy caused by the different location of the O-vacancy from those introduced by the presence of neighboring O-vacancies, in a growing O-vacancy island, which was not possible in earlier calculations.[20;21] The driving force for the formation of O-vacancy islands was calculated by consecutive removal of neighboring O-atoms in the lattice, both in the presence and in the absence of the Ru nanorod. Furthermore, we now included not only surface vacancy islands underneath the Ru nanorod (removal of O-atoms from 1i to 5i in Figure 2c), but also surface O-vacancy islands aside the Ru nanorod, formed by sequential removal of O-atoms 1i, 17i, 18i, and 14i, and finally vertical O-vacancy islands underneath the edge of the Ru nanorod created by consecutive removal of O atoms 1i, ii, iii and iv.

To further identify and characterize correlations between CO adsorption strength and the electronic properties of the Ru adsorption site, we calculated the local density of d-states (LDOS) at these Ru atoms, using a 17×3×1 k-point mesh, where the Ru nanorod extends in the x-direction (Fig. 2b).

The energy for the formation of an (additional) O-vacancy, E_f, in the fully oxidized, bare $ZrO_2(111)$ support and in the Ru/ZrO_2 model system, and the effect of the Ru nanorod on the vacancy formation energy, $\Delta E_{vac.stab.}$, were calculated, respectively, via equations (1) – (3)

$$E_{vac,ZrO2}(x) = E_{ZrO2-x} - E_{ZrO2-(x-1/n)} - {}^1/_2\, E_{O2} \quad (1)$$

$$E_{vac,Ru/ZrO2}(x) = E_{Ru-ZrO2-x} - E_{Ru-ZrO2-(x-1/n)} - {}^1/_2\, E_{O2} \quad (2)$$

$$\Delta E_{vac}(x) = E_{vac,Ru/ZrO2}(x) - E_{vac,ZrO2}(x) \quad (3)$$

Here x again denotes the number of O-vacancies, including the newly formed one, and E_{O2} refers to the DFT calculated energy of the O_2 molecule. n is the number of ZrO_2 units per Ru/ZrO_2 unit cell

3 Results and Discussion

3.1 Vacancy formation energies

In this part, we calculated the energy required for the formation of O-vacancies in a ZrO_2 support, both as individual O-vacancies and as part of a growing O-vacancy cluster in the presence and in the absence of a Ru nanorod. We considered various positions in the top layer and also positions in deeper layers of the ZrO_2 support. Furthermore, we explored the relationship between the reduction in O-vacancy formation energy caused by the presence of the Ru nanorod and the charge transfer from the support to the Ru nanorod upon O-vacancy formation. We will demonstrate that there is an approximately linear relationship between the Ru-induced lowering of the O-vacancy formation energy and the charge transfer from the support to the Ru nanorod upon O-vacancy formation. This will be discussed for different types of O-vacancies, at the interface directly underneath the Ru nanorod, in the top-layer aside the Ru nanorod, and in deeper layers underneath the Ru nanorod, as well as for individual O-vacancies and O-vacancy clusters.

3.1.1. Formation of O-vacancies directly underneath the Ru nanorod

Formation of individual O-vacancies: In a first step, we calculated the energy costs for the removal of an individual surface O atom (O-vacancy formation energy, E_{vac}) at different positions underneath the Ru nanorod, to gain an impression of the variation in these values, both in the absence and in the presence of the Ru nanorod. This differs from our previous work,[21] where we had calculated the formation energy for an O-vacancy at a specific interface site at the edge of the Ru nanorod (interface perimeter site) in a stepwise increasing O-vacancy cluster. The O-vacancy formation energies obtained for nine different surface oxygen sites (1i to 9i), all of which are located underneath the Ru nanorod (Figure 2c), are illustrated by the colored bars in Figure 3a for the bare ZrO_2 (pink bars) and for the Ru/ZrO_2 model system (grey bars), respectively. The respective energies and the resulting differences are summarized also

in Tables S1, S2 and S3 in the Supporting Information (SI). Common trend of these data is that the O-vacancy formation energies differ rather little relative to their total value, varying by at most 0.7 eV, for the different sites on the bare ZrO_2 support. In contrast, the variations are significantly more pronounced, up to ~2.5 eV, for the Ru/ZrO_2 model systems.

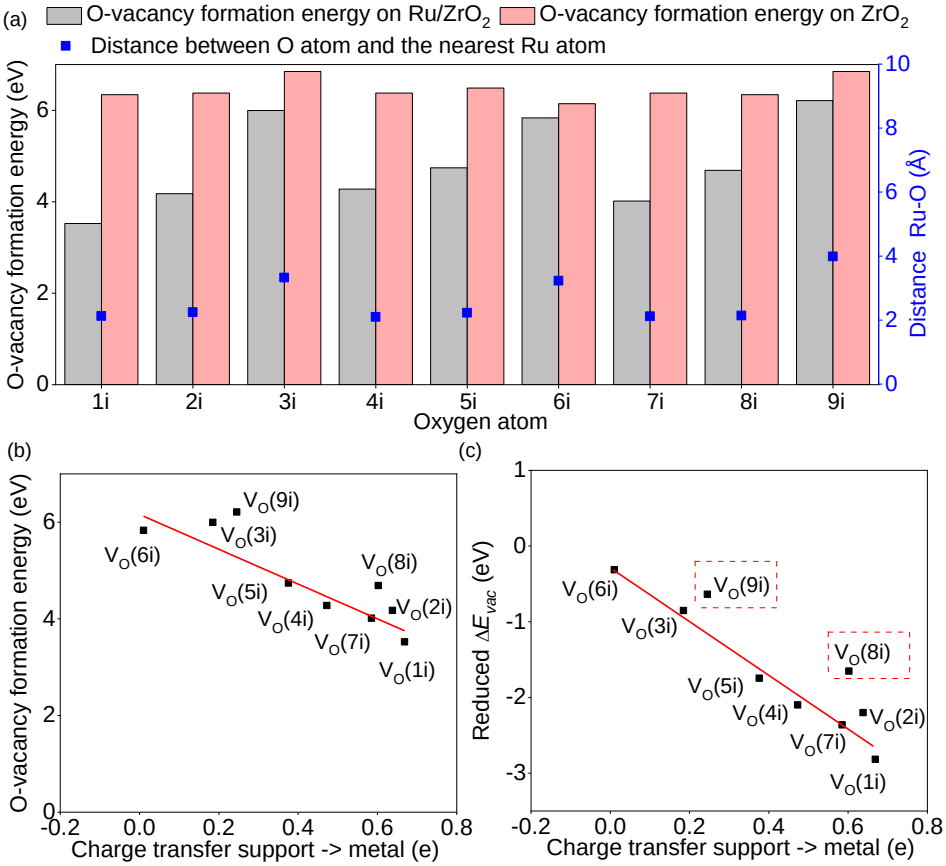

Figure 3 (a) Energies for the formation of individual O-vacancies on different interface sites (1i to 9i, see Figure 2c) on the fully oxidized, relaxed ZrO_2 (pink bars) and Ru/ZrO_2 model systems (grey bars). Blue dots indicate the distance between the O-vacancy and the closest Ru atom. (b) Plot of the O-vacancy formation energies on the different sites of Ru/ZrO_2 vs. the charge transfer from the support to the Ru nanorod upon O-vacancy formation. V_O(ni) (n=1-9) etc. denote the O-vacancy formation at the site ni on Ru/ZrO_2. The full line is a fit to the data points V_O(1i) – V_O(7i) (see below). (c) Corresponding data for the Ru-induced lowering of the O-vacancy formation energy ΔE_{vac} on Ru/ZrO_2.The full lines are fits to the data points V_O(1i) – V_O(7i), i.e., all points except those marked by a dashed red square, which exhibit

structural contributions ($E_{Ru}^{deform} + E_{support}^{deform}$) of 0.29 eV or more (see text and Table S4).

A more detailed inspection reveals that the O-vacancy formation energies in Ru/ZrO_2 seem to be correlated with the distance between the O-vacancy and the nearest Ru atom, where the latter are indicated by blue dots in Figure 3a. As an example, for the 9i, 3i and in particular for the 6i sites, where the distances to the nearest Ru atom are above 3 Å, the energy costs for O-vacancy formation in the presence of the Ru nanorod are closer to those on ZrO_2 alone, with energy differences within 0.8 eV. In contrast, for the 1i, 2i, 4i, 5i, 7i, and 8i O-atoms, where the shortest distances to a neighboring Ru atom are around 2 Å, the reduction of the O-vacancy formation energy induced by the Ru nanorod is more than 1.50 eV. Apparently, this distance is a decisive parameter for the Ru nanorod induced promotion of the O-vacancy formation, although there is no linear correlation between these parameters. Sizeable effects can be expected if the distance to the closest Ru atom is around 2 Å. For comparison, the Ru-O bond length in rutile RuO_2 is about 1.49 Å.

Charge transfer upon O-vacancy formation: Previously we had reported that the formation of O-vacancies is accompanied by a partial reduction of the neighboring Zr ions and, in the presence of the Ru nanorod, by a less pronounced reduction of the Zr ions and an electron transfer from the support to the Ru nanorod.[21] Regarding the partial reduction of the Zr ions adjacent to the O-vacancy one should keep in mind, however, that the charge partitioning procedure assigns the electron charge in the O-vacancy region to the neighboring ions. Nevertheless, in the presence of the Ru nanorod, the reduction of the Zr ions adjacent to the O-vacancy is less pronounced, leading to a lower energy cost for O-vacancy formation. Actually, there seems to be an essentially linear relation between the O-vacancy formation energy E_{vac} on the one hand and the charge transfer from the support to the Ru nanorod upon O-vacancy formation on the other hand, with more charge transfer going along with a lower O-vacancy

formation energy (Figure 3b). The correlation is even more obvious when plotting the Ru-induced lowering of the O-vacancy formation energy ΔE_{vac} rather than the O-vacancy formation energy itself versus the charge transfer from the support to the Ru nanorod upon O-vacancy formation (Figure 3c). In this case, effects from structural differences between the different oxygen sites in the Ru-free ZrO_2 surface should be largely cancelled. Indeed, except for the data points 2i, 8i and 9i, there is a strict correlation between the Ru-induced lowering of the O-vacancy formation energy and the charge transfer, which is indicated by the full line (see also the following discussion).

To identify possible reasons for the less pronounced Ru-induced lowering of the O-vacancy formation energy ΔE_{vac} at the sites 2i, 8i and 9i, we decomposed the Ru-induced change in vacancy formation energy ΔE_{vac} into contributions arising from changes in the interaction between the Ru nanorod and the support ($\Delta E^{int}_{Ru-support}$), while maintaining the previous structure, i.e., without any structural modification, and contributions resulting from the structural modification of the Ru nanorod, E^{deform}_{Ru}, and of the support, $E^{deform}_{support}$, which are induced by the presence of the O-vacancy:

$$\Delta E_{vac} = \Delta E^{deform}_{Ru} + \Delta E^{deform}_{support} + \Delta E^{int}_{Ru-support} \quad (4)$$

This approach, which is based on ideas outlined in our previous work,[21] but differs in details, is described and illustrated in the schematics in Figure S1. In short, $\Delta E^{int}_{Ru-support}$ can be calculated as the difference in interaction energy in the relaxed Ru/ZrO_2 model catalyst and in the relaxed Ru/ZrO_{2-x} model catalyst, with the (additional) O-vacancy, where the interaction energy is calculated as the energy difference between the complete system and the separate components, while maintaining their structure. ΔE^{deform}_{Ru} corresponds to the energy required for changing the structure of the separate Ru nanorod from that in the relaxed Ru/ZrO_2 to that in the relaxed Ru/ZrO_{2-x} system, after creation of an O-vacancy in the support. Accordingly,

$\Delta E_{support}^{deform}$ can be calculated as the energy required for changing the structure of the separate ZrO_2 support from that in the relaxed Ru/ZrO_2 to that in the relaxed Ru/ZrO_{2-x} system. Furthermore, it also contains the difference in energy for the removal of an O-atom (see Figure S1). Splitting this up into separate contributions would be ambiguous, since depending on whether the O-removal would take place before or after restructuring the resulting numbers would be different. As illustrated in the reaction cycle in Figure S1, the O-vacancy formation energy in the ZrO_2 support cancels out, since we are considering the difference in O vacancy formation energy ΔE_{vac} between the Ru/ZrO_2 model catalyst and the pure ZrO_2 support, rather than the O-vacancy formation energy E_{vac} itself.

The sums of the structural contributions (ΔE_{Ru}^{deform} and $\Delta E_{support}^{deform}$) and the differences in interaction energies ($\Delta E_{Ru-support}^{int}$) calculated for the formation of a single O-vacancy at different sites are listed in Table S4. Obviously, in all cases the difference in interaction energy is the dominant contribution to the Ru-induced lowering of the O-vacancy formation energy. In many cases, the interaction energy is by about 2.0 eV more negative for the Ru/ZrO_{2-x} system than for the Ru/ZrO_2 system, leading to a corresponding stabilization of the O-vacancy by the Ru nanorod. In contrast, the structural contribution is generally rather low. This is particularly true for the Ru deformation energy ΔE_{Ru}^{deform}, which except for few exceptions is below +0.1 eV.

It is obvious, that the two data points with the largest deviation from the red line in Figure 3c, V_O(8i) and V_O(9i), are also those with the largest structural contribution, underlining that the structural contribution has an important effect on this deviation. For illustration, we marked all data points with medium or high structural contributions (≥ 0.29 eV) with a red dashed rectangle. On the other hand, a simple correlation between the size of the deviation from a linear relationship between the O-vacancy formation energy change caused by the Ru nanorod and

the Ru-support charge transfer, which is indicated by the red line, and the contribution from restructuring effects (structural contribution) is not possible. Furthermore, these structural contributions are an important, but not the only effect that can result in a sizable deviation of a data point from the linear correlation indicated by the red line. This is illustrated, e.g., by the O-vacancy formation on the 2i site, where the structural contribution is very small (see Table S4). These questions will be investigated in more detail in future work. Nevertheless, despite these deviations, the energy required for O-vacancy formation depends mainly on the feasibility of charge transfer from the support to the Ru nanorod upon vacancy formation, and this in turn depends mainly on the distance between O-vacancy and the closest Ru atom.

Finally, we would like to note that these arguments and considerations refer to the energetics of the O-vacancy formation process, where additional kinetic barriers are not included. Most important, kinetically the exchange at the perimeter of the interface will be favored as compared to O-vacancy formation on more central sites underneath the Ru nanorod. Formation of O-vacancies underneath the Ru nanorod is only possible via subsequent migration of interface perimeter O-vacancies, e.g., at elevated temperatures.

Formation of O-vacancies in a growing O-vacancy cluster: Next, we calculated the formation energy of O-vacancies at the same sites underneath the Ru nanorod as before, but now in a growing two-dimensional (2D) O-vacancy cluster. Following the first O-vacancy formation at the 1i site, additional O-vacancies were generated at neighboring oxygen sites (from the 2i, 3i, 4i to the 5i site), finally resulting in an O-vacancy cluster with five adjacent O-vacancies. In Figure 4a we compare the energy cost for the formation of an additional O-vacancy in the growing cluster (blue bars) with that of a single, isolated O-vacancy at the same site (grey bars). The data are also listed in Table S1. In most of the cases, the energy cost for the O-vacancy formation in the cluster is lower than or equal to that for the formation of an isolated vacancy, but the differences are generally small. They are most pronounced for the

energetically most costly O-vacancy formation at the 3i and 5i sites, where the differences are 0.38 and 0.44 eV, respectively. Hence, promotional effects induced by the presence of neighboring O-vacancies are generally small. A similar trend is also observed for the formation of an O-vacancy in a growing cluster in the absence of a Ru nanorod (see Table S2). The only exception in these sequences is the formation of the third O-vacancy at the 3i site in a cluster, which is by 0.83 eV less costly than that of an isolated vacancy at that site.

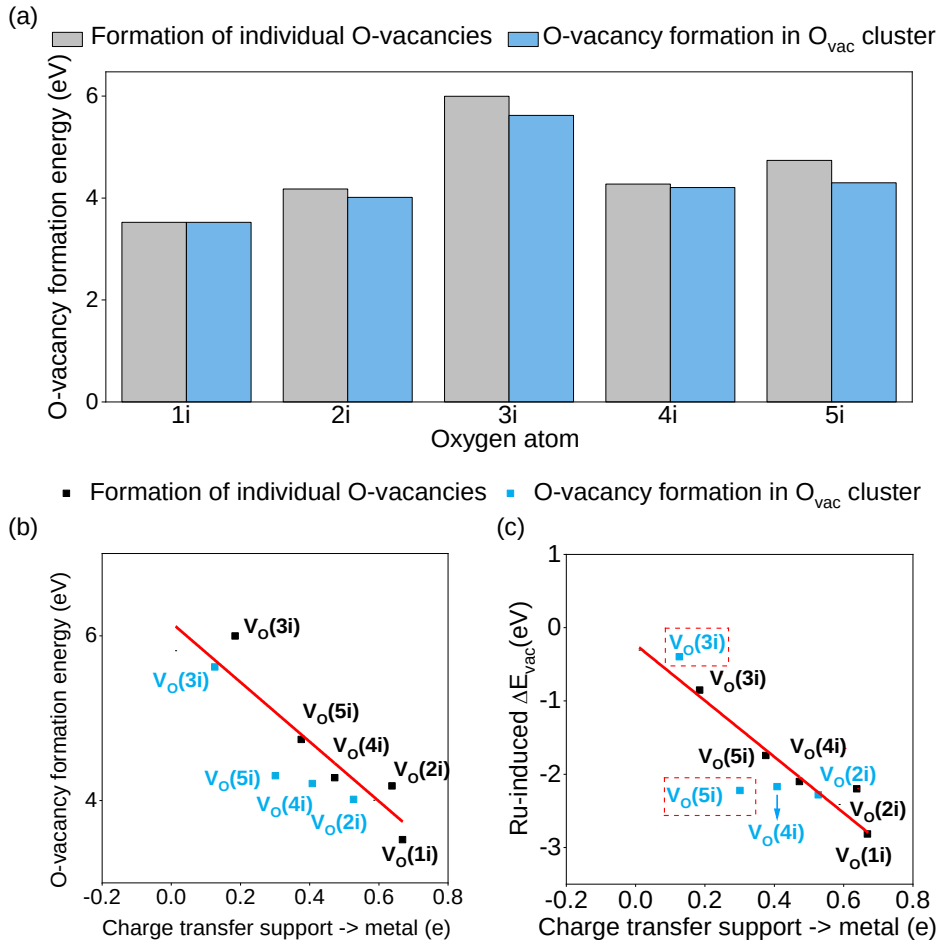

Figure 4. (a) Energies for the formation of individual O-vacancies at the sites indicated on fully oxidized Ru/ZrO_2 (grey bars) and of O-vacancies in a growing 2D O-vacancy cluster on sites 1i → 5i on fully oxidized Ru/ZrO_2 (1i) / partly reduced Ru/ZrO_{2-x} (blue bars). (b) O-vacancy formation energy ΔE_{vac} on Ru/ZrO_2 as a function of the charge transfer from the support to the Ru nanorod upon O-vacancy formation for individual O-vacancies (black symbols) and for O-vacancy formation in a growing 2D O-vacancy cluster (blue symbols). (c) Corresponding data for the Ru-induced

lowering of the O-vacancy formatin energy ΔE_{vac} on Ru/ZrO_2. The red lines represent the fits to the data in Figure 3b and 3c, the data points within the red dashed rectangles have structural contributions ($\Delta E_{Ru}^{deform} + \Delta E_{support}^{deform}$) of 0.29 eV or more.

As before, we also plotted the relation between the O-vacancy formation energy E_{vac} and the charge transfer from the support to the Ru nanorod upon O-vacancy formation in the growing O-vacancy cluster (blue squares in Figure 4b) and the relation between Ru-induced lowering of the O-vacancy formation energy ΔE_{vac} and the above charge transfer (blue squares in Figure 4c). For comparison, we also included the corresponding data for individual O-vacancies from Figure 3b and 3c (black dots). In all cases, the additional charge transfer upon formation of an O-vacancy in a growing O-vacancy cluster is smaller than that for the individual vacancy at the same location, which can be understood based on depolarization effects. (Note that this comparison is only possible for the vacancies V_O(2i) – V_O(5i)). Except for this depolarization effects and the resulting shift to lower charge transfer, the data points seem to fit reasonably well to the linear correlations derived in Figure 3b and 3c, which are included as red lines. Hence, the linear relation between charge transfer and Ru-induced lowering of the O-vacancy formation energy, which was derived for the formation of individual O vacancies, is also applicable to O-vacancy formation in a cluster. For the V_O(5i) vacancy, where the O-vacancy formation energy and the Ru-induced lowering of it are significantly lower than expected from the linear regression, the structural contribution ($\Delta E_{Ru}^{deform} + \Delta E_{support}^{deform}$) (Table S5) is significantly higher than for the V_O(2i) and V_O(4i) O-vacancies, supporting the role of restructuring effects as discussed before. On the other hand, these deviations (Figure 4b and 4c) are much smaller for the V_O(3i) site, supporting our above suggestion that larger structural contributions are an important, but not the only possible origin for a significant deviation from the linear relation between charge transfer and Ru-induced stabilization of an O-vacancy.

3.1.2 Formation of surface O-vacancies aside the Ru nanorod

Next, we explored in a similar approach the formation of individual surface O-vacancies and surface O-vacancies in a growing 2D cluster, where either all O-vacancies or most of them are aside the Ru nanorod.

Formation of individual O-vacancies aside the Ru nanorod: First we present the vacancy formation energies for removing individual O surface atoms at positions 13i to 18i aside the Ru nanorod (see Figure 2c). We disregarded the 10i - 12i sites, since they are located underneath the interface perimeter, similar to the 1i - 3i oxygen atoms. From these sites, 16i – 18i and in particular 16i and 17i are closer to the edge of the Ru nanorod and therefore termed as first row sites, while sites 13i – 15i are further apart (second row). O-vacancy formation energies obtained for the bare ZrO_2 system and on the Ru/ZrO_2 model system are plotted in Figure 5a (see also Tables S1and S2), the distance to the nearest Ru atom is again indicated by blue squares. First of all, the data clearly demonstrate very small difference between O-vacancy formation energies on ZrO_2 and Ru/ZrO_2 for these positions without direct contact with Ru atoms, with distances between O-vacancy and nearest Ru atom from 3.82 to 7.33 Å. This is equivalent to a rather small Ru-induced stabilization of the O-vacancies on these sites. It fits to our previous general conclusion (section 3.1.1) that a significant lowering of the O-vacancy formation energy by the Ru nanorod is only possible if the distance to the nearest Ru atom is short, on the order of 2 Å. The higher energy level of these vacancies aside the Ru nanorod compared to O-vacancies directly underneath the Ru nanorod, i.e., at interface sites, also means that they are much less probable than the latter ones.

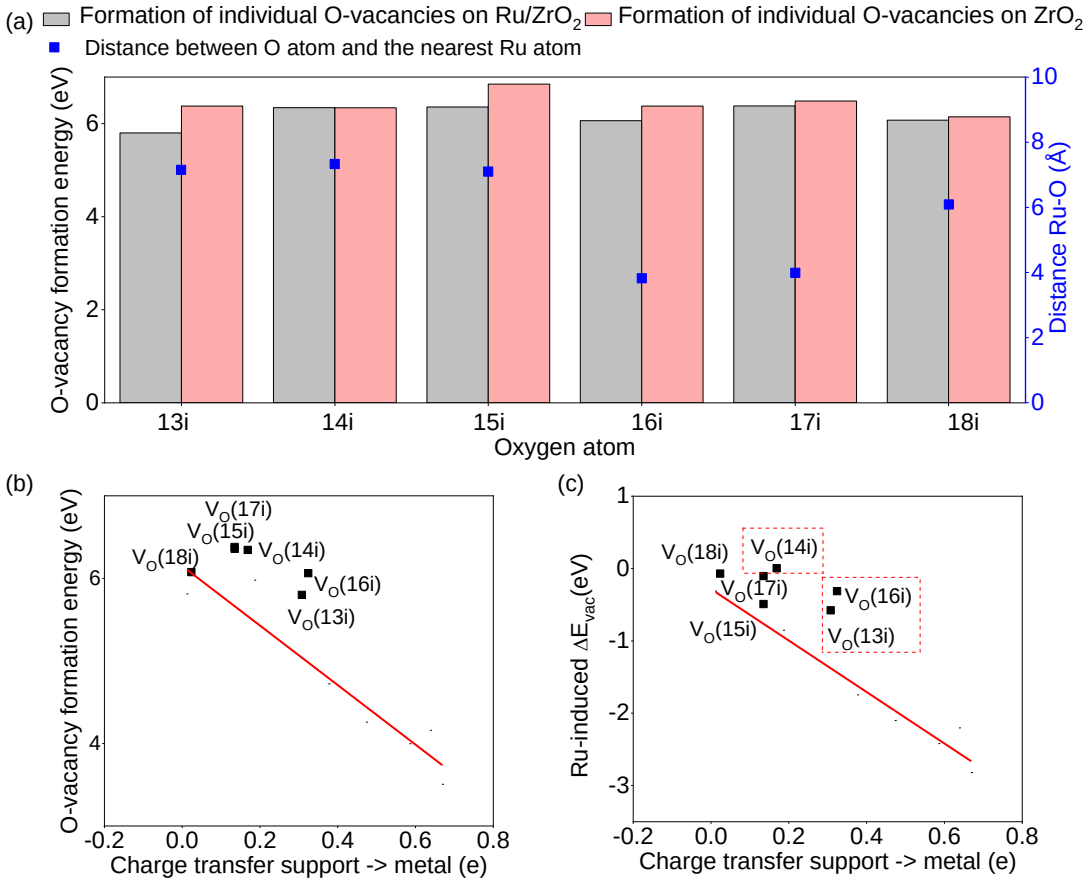

Figure 5. (a) Energies for the formation of individual O-vacancies at different sites aside the Ru nanorod (13i to 18i, see Figure 2c) on the fully oxidized, relaxed ZrO_2 (pink bars) and on the fully oxidized, relaxed Ru/ZrO_2 model system (grey bars). Blue squares indicate the distance between O-vacancy and the nearest Ru atom. (b) Plot of the O-vacancy formation energies on the different sites of Ru/ZrO_2 vs. the charge transfer from the support to the Ru nanorod upon O-vacancy formation. Note that we used the same scale as in Figure 3 to better illustrate the spread in the data points (c) Corresponding data for the Ru-induced lowering of the O-vacancy formation energy ΔE_{vac} on Ru/ZrO_2. V_O (ni) (n=13-18) denote the O-vacancy formation at the site ni on Ru/ZrO_2 (Figure 2c). The red lines represent the fits to the data in Figure 3b and 3c, the data points within the red dashed rectangles have structural contributions ($\Delta E_{Ru}^{deform} + \Delta E_{support}^{deform}$) of 0.29 eV or more.

Possible correlations between the charge transfer from the support to the Ru nanorod and the O-vacancy formation energy or the Ru-induced lowering of that quantity are illustrated in Figure 5b and 5c, respectively (see also Table S4). Also for these sites there is still some charge

transfer possible, up to above 0.32 electrons (16i), while the effect on the Ru-induced lowering of the O-vacancy formation energy is only very limited (Figure 5c). As a result, all of these data points lie above the red line reflecting the linear correlation between charge transfer from the support to the Ru nanorod upon O-vacancy generation and the Ru-induced lowering of the O-vacancy formation energy deduced in Figure 3c. However, the O-vacancy induced charge transfer cannot be easily correlated with the distance to the closest Ru atom (Figure 5a). As an example, the charge transfer upon O-vacancy formation at the 13i site is significantly larger than that upon O-vacancy formation on the 17i site (Figure 5b and 5c), despite the larger distance to the closest Ru atom. This supports our earlier conclusion that the correlation between charge transfer upon O-vacancy formation and Ru-O distance is more qualitative, with significant charge transfer and energy effects only for distances about 2 Å, while at larger distances the O-vacancy stabilization becomes significantly smaller and more dominated by local effects (see section 3.1.1). Such effects may include, e.g., structural contributions as discussed before, which are generally more pronounced than those from vacancies underneath the Ru nanorod (Table S4). For instance, they are higher for the V_O(13i) and V_O(16i) vacancies (marked by a red square), in agreement with our suggestion that the less pronounced Ru-induced lowering of the O-vacancy formation energy is at least partly due to structural factors. On the other hand, for the V_O(15i) vacancy, which also shows a significant deviation from this linear correlation, the structural contribution is even negative and of similar size as the difference in interaction energies (Table S4). This supports our previous conclusion that these structural contributions are one, but not the only important contribution to deviations from this linear correlation.

In general, when the O-vacancy is located close to but not in direct contact with the Ru nanorod, there is significantly less charge transfer between the Ru nanorod and a lower Ru-induced

stabilization of the O-vacancy. This is often connected with a greater influence from local, structural contributions.

Formation of O-vacancies in a growing O-vacancy cluster: Similar to section 3.1.1, we also determined the O-vacancy formation energies in a growing 2D vacancy cluster, which is formed by the stepwise removal of lattice O atoms from site 1i via sites 17i, 18i to finally 14i, where the latter three are located aside the Ru nanorod. Note that due to the periodicity of the system the O-atom 14i is neighbored to atoms 17i and 18i. Figure 6a (see also Table S1) shows the resulting O-vacancy formation energies (blue bars) and those obtained for individual O-vacancies at the same locations (grey bars), where the latter were presented already in Figure 5a. Similar to the general trend obtained for O-vacancy formation underneath the Ru nanorod, the removal of lattice O-atoms costs slightly less energy in the presence of the neighboring O-vacancies than for the isolated O-vacancies. In the present case, the differences are even smaller, and therefore, if formed, O-vacancy clusters can co-exist with the individual O-vacancies in the surface layer (see also Table S1 and S2).

In Figure 6b we illustrate the relationship between the O-vacancy formation energy and the charge transfer from the support to the Ru nanorod upon the formation of O-vacancies in a growing 2D O-vacancy cluster (blue squares). Figure 6c presents a similar plot of the Ru-induced lowering of the O-vacancy formation energy ΔE_{vac} (blue squares). For comparison, the data for individual O-vacancies (black squares) are included as well in these figures. For these O-vacancies the charge transfer from the support to the Ru nanorod upon O-vacancy formation is very small (< 0.2 electrons per new O-vacancy), and except for the V_O(14i) vacancy, very close to that in the individual O-vacancies. For the V_O(14i) cluster vacancy, the charge transfer is about 0.15 e less than for the formation of an individual O-vacancy, which would again be consistent with a depolarization effect. The Ru-induced lowering of the O-vacancy formation energies ΔE_{vac} for the $1V_O$ – $3V_O$ systems, which is anyway very small, is only little affected

by the presence of the neighbored O-vacancies, mostly by around 0.1 eV. The highest energy deviation from the linear correlation between charge transfer and Ru-induced O-vacancy stabilization is observed for the 17i site, which also shows the highest structural contribution (Table S5, marked by a red rectangle in Figure 6c). This agrees well with the significant deviation from this linear regression for the O-vacancy formation at the 17i site, supporting our previous suggestion that such deviations are particular likely for higher structural contributions. In contrast, these contributions are smaller for the 14i and 18i sites (Table S5), in agreement with the lower magnitude of the Ru-induced stabilization for O-vacancies at these sites.

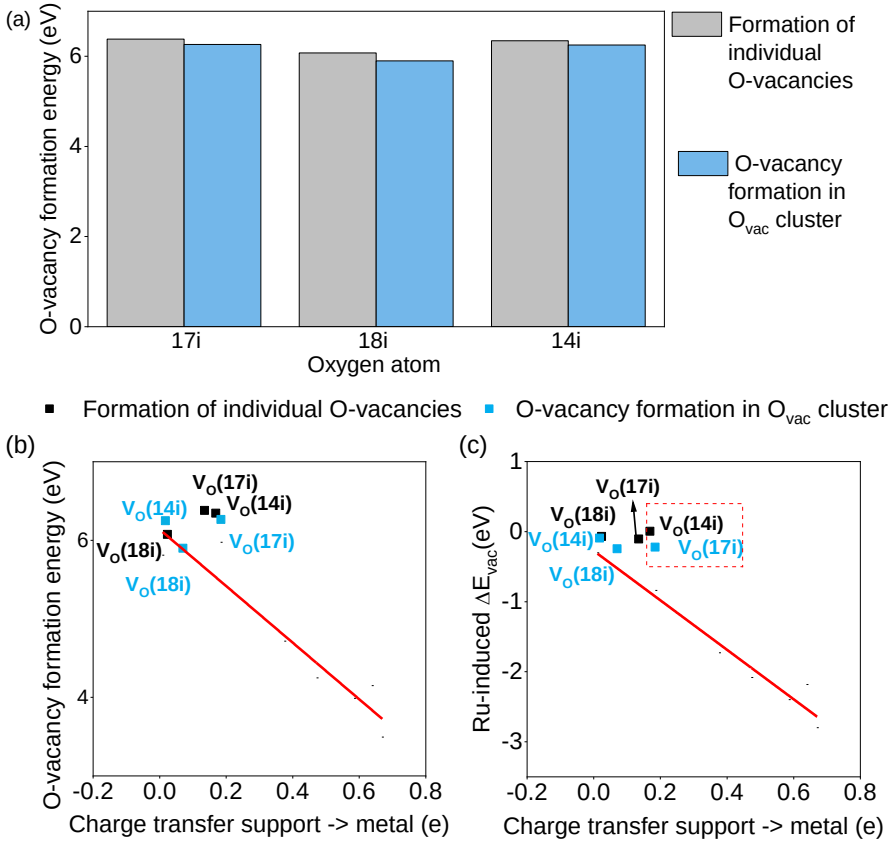

Figure 6. (a) Energy for the formation of an individual O-vacancy at the site indicated on fully oxidized Ru/ZrO_2 (grey bars) and in the presence of neighboring O-vacancies in a growing 2D O-vacancy cluster on partly reduced Ru/ZrO_{2-x} (blue bars) as a function of the position of the O-vacancy from 1i (not shown) via 17i, 18i to 14i. (b) Plot of the O-vacancy formation energies on Ru/ZrO_2 for O-vacancies in a 2D O-vacancy cluster (blue squares) and, for comparison, for individual O-vacancies (black squares)

vs. the charge transfer from the support to the Ru nanorod upon O-vacancy formation. (c) Corresponding data for the Ru-induced lowering of the O-vacancy formation energy ΔE_{vac} on Ru/ZrO_2. $V_O(ni)$ (n= 17, 18,14) denote the O-vacancy formation at the site ni on Ru/ZrO_2 and Ru/ZrO_{2-x} (Figure 2c). The red lines represent the fits to the data in Figure 3b and 3c, the data points within the red dashed rectangles have structural contributions ($\Delta E_{Ru}^{deform} + \Delta E_{support}^{deform}$) of 0.29 eV or more.

3.1.3. Formation of O-vacancies in deeper layers underneath the Ru nanorod

Formation of individual O-vacancies: Diffusion of O-vacancies from the top layer to deeper layers of the support may allow O-vacancy formation also in deeper layers. Therefore, we also calculated the O-vacancy formation energies in deeper layers underneath the interface perimeter sites, on sites ii, iii, and iv. Energies for O-vacancy formation on these sites (see Figure 2c) were calculated for the pure support ZrO_2 and for the Ru/ZrO_2 model system. These oxygen atoms were found to be most favorable for O-vacancy formation in the respective layers. The resulting energies are displayed in Figure 7a (see also Table S1 and S2), together with the distance between O-vacancy and the nearest Ru atom (blue squares). Different from the O-vacancy in the topmost layer (site 1i, see Figure 3a), the influence of the Ru-nanorod on the vacancy formation energy is very small (-0.4 eV at site iii) or negligible (other sites) (Figure 7a). Hence, the Ru-induced lowering of the O-vacancy formation energy is essentially limited to O-vacancy generation in the topmost layer, with direct contact to the Ru nanorod. The slight stabilization of the O-vacancy in the third layer (site iii) seems to be related to a higher charge transfer (see below), indicating that in addition to the distance to the nearest Ru atom also other, local effects can play a role, though the latter is by far the most dominant factor. This will be discussed further in the next paragraph.

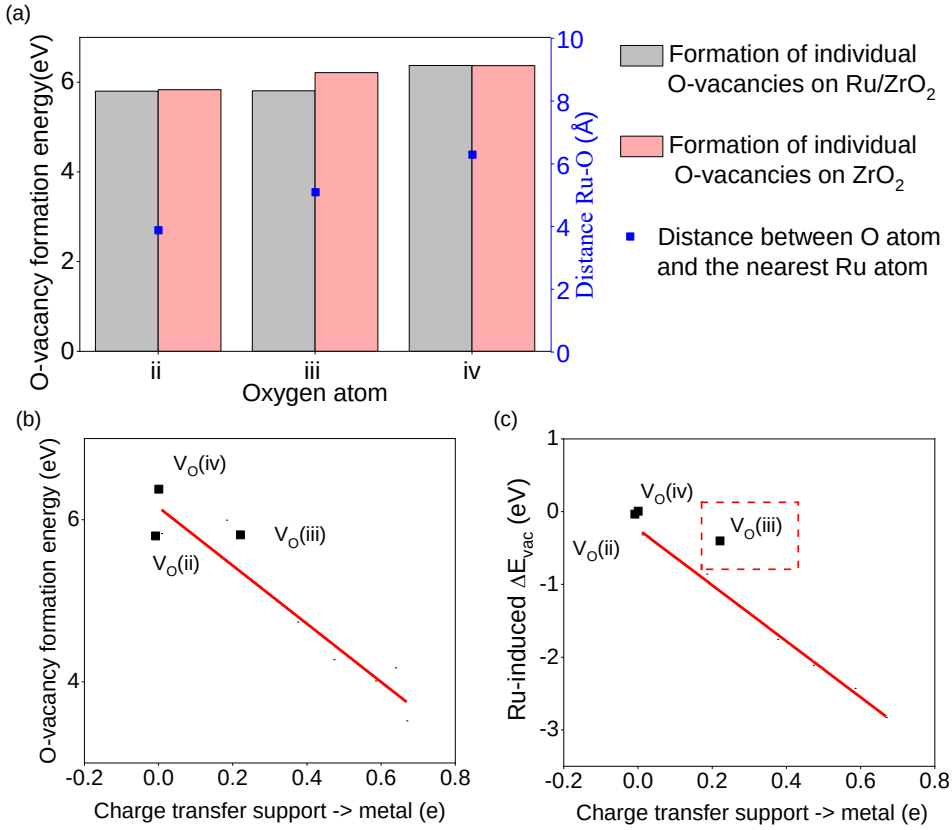

Figure 7. (a) Energy for the formation of a single isolated O-vacancy in deeper layers (2nd to 4th layer, on ii, iii and iv sites, see Figure 1c) on fully oxidized Ru/ZrO_2 (grey bars) and ZrO_2 (red bars). Distances between O-vacancy and the nearest Ru atom are indicated by blue squares. (b) Plot of the O-vacancy formation energy E_{vac} for isolated O-vacancies on Ru/ZrO_2 in deeper layers (black squares) vs. the charge transfer from the support to the Ru nanorod upon O-vacancy formation. (c) Corresponding data of the Ru-induced lowering of the O-vacancy formation energy ΔE_{vac} on Ru/ZrO_2. V_O (i) – V_O(iv) denote the O-vacancy formation at the respective sites of Ru/ZrO_2 (Figure 2c). The red lines represent the fits to the data in Figure 3b and 3c, the data points within the red dashed rectangles have structural contributions ($\Delta E_{Ru}^{deform} + \Delta E_{support}^{deform}$) of 0.29 eV or more.

Plots of the O-vacancy formation energy E_{vac} and the Ru-induced lowering of the O-vacancy formation energy ΔE_{vac} on Ru/ZrO_2 against the charge transfer from the support to the Ru nanorod upon O-vacancy formation are shown in Figure 7b and 7c, respectively. While in two cases, V_O(ii) and V_O(iv), the charge transfer is negligible, there is still some charge transfer to

the Ru nanorod for the V_O(iii) vacancy formation, despite the distance of about 5 Å to the nearest Ru atom. We tentatively rationalize this charge transfer upon O-vacancy formation at the iii site by the direct contact between the Zr ion above the O-vacancy (4Zr) and the Ru atom 2a (distance 2.20 Å), which seems to promote the electron transfer and thus vacancy formation compared to the ZrO_2 support (Figure 7a). In contrast, although the O-vacancy at the ii site is close to the 3Zr ion with a distance of 2.17 Å, the 3Zr ion does not interact directly with a neighboring Ru atom (1a), but via the uppermost lattice O atoms. Consequently, the lack of direct contact between the Ru atom 1a and the 3Zr ion (distance 2.86 Å) at the ii site results in almost no charge transfer. Thus, in specific cases charge transfer between the support and the Ru nanorod can also occur via direct contact between a Ru atom and a Zr ion neighboring an O-vacancy.

Similar to O-vacancy formation aside the Ru nanorod, also in this case the Ru-induced lowering of the O-vacancy formation energy is less than expected from the linear correlation between Ru-induced lowering of the O-vacancy formation energy and the charge transfer from the support to the Ru nanorod derived in Figure 3c (red line in Figure 7c). This is particularly evident for O-vacancy formation at the (iii) site. Again, the structural contribution is much higher, by about 1.0 eV, than in the other cases (marked by a red dashed rectangle in Figure 7c, see also Table S4), supporting again our suggestion that significant structural contributions to the O-vacancy formation energy generally result in more pronounced deviations from the linear correlation between the O-vacancy induced charge transfer to the Ru nanorod and the Ru-induced lowering of the O-vacancy formation energy.

Formation of O-vacancies in a vertical O-vacancy cluster: Finally, we also calculated the effect of neighboring O-vacancies on the O-vacancy formation energy at the ii, iii, and iv sites, i.e., on the O-vacancy formation in a growing 2D vacancy cluster for comparison (see Table S1). Starting with an O-vacancy at the 1i site (see Figure 3), we sequentially added neighboring

O-vacancies at the ii, iii and iv sites. The resulting vacancy formation energies are essentially identical to those obtained for isolated O-vacancies on these sites, with differences of at most 0.10 eV (Figure 8a). Hence, also in this case the presence of neighboring O-vacancies does not significantly ease the formation of O-vacancies in deeper layers. Plotting the O-vacancy formation energy vs. the charge transfer upon O-vacancy formation (blue symbols, Figure 8b), the data are rather close to those obtained for the formation of individual O-vacancies (black symbols), both in charge transfer and in the O-vacancy formation energy. The same is true also for the Ru-induced lowering of the O-vacancy formation energy (Figure 8c). Similar to the individual O-vacancies, also in this case all data points are located above the fit line derived in Figure 3c. Hence, depolarization effects paly a negligible role in these clusters.

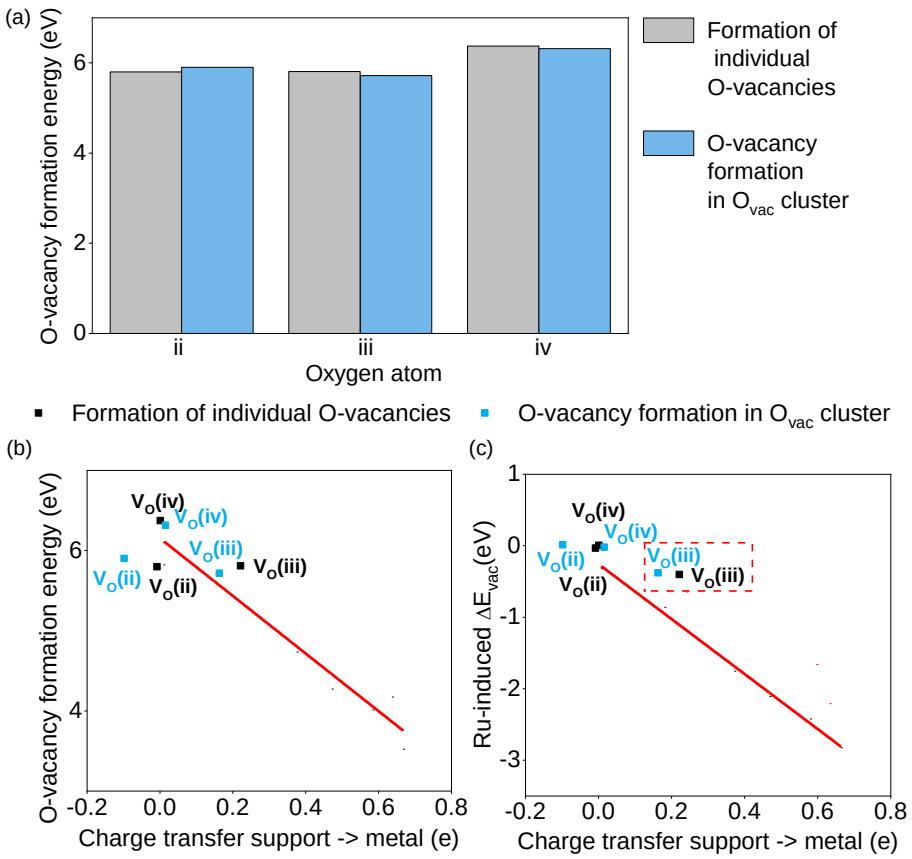

Figure 8. (a) Energy for the formation of an individual O-vacancy at the site indicated on fully oxidized Ru/ZrO_2 (grey bars) and in the presence of neighboring O-vacancies in a growing 2D O-vacancy cluster on partly reduced Ru/ZrO_{2-x}, with the first O-vacancy on the 1i site (blue bars) as a function of the position of the O-vacancy

from ii via iii to iv. (b) Plot of the O-vacancy formation energies E_{vac} on Ru/ZrO_2 for O-vacancies in a 2D O-vacancy cluster in deeper layers (blue squares) and for comparison, for individual O-vacancies (black squares) vs. the charge transfer from the support to the Ru nanorod upon O-vacancy formation. (c) Corresponding data for the Ru-induced lowering of the O-vacancy formation energy ΔE_{vac} on Ru/ZrO_2. V_O(ii) – V_O(iv) denote the O-vacancy formation at the respective sites (from ii to iv in Figure 2c) on Ru/ZrO_{2-x}. The red lines represent the fits to the data in Figure 3b and 3c, the data points within the red dashed rectangles have structural contributions ($\Delta E_{Ru}^{deform} + \Delta E_{support}^{deform}$) of 0.29 eV or more.

Correlation between Charge Transfer upon O-vacancy Formation and O-Vacancy Formation Energy

Combining the data presented in the previous sections, we obtain a broader trace of data points, which lie along the linear relation between charge transfer upon O-vacancy formation and the Ru-induced lowering of the O-vacancy formation energy derived in Figure 3c for O-vacancies in direct contact with the Ru nanorod. The charge transfer was shown to be qualitatively correlated with the distance between O-vacancy and the nearest Ru atom, resulting in significant charge transfer only for distances around 2.0 Å. This is only possible for O-vacancies in the interface layer. But also other, more local effects can play a role, though on a smaller scale, one examples for this is a charge transfer mediated by a close, direct contact between a Zr ion neighbored to the O-vacancy and a Ru interface atom, which allows some charge transfer also for larger distances.

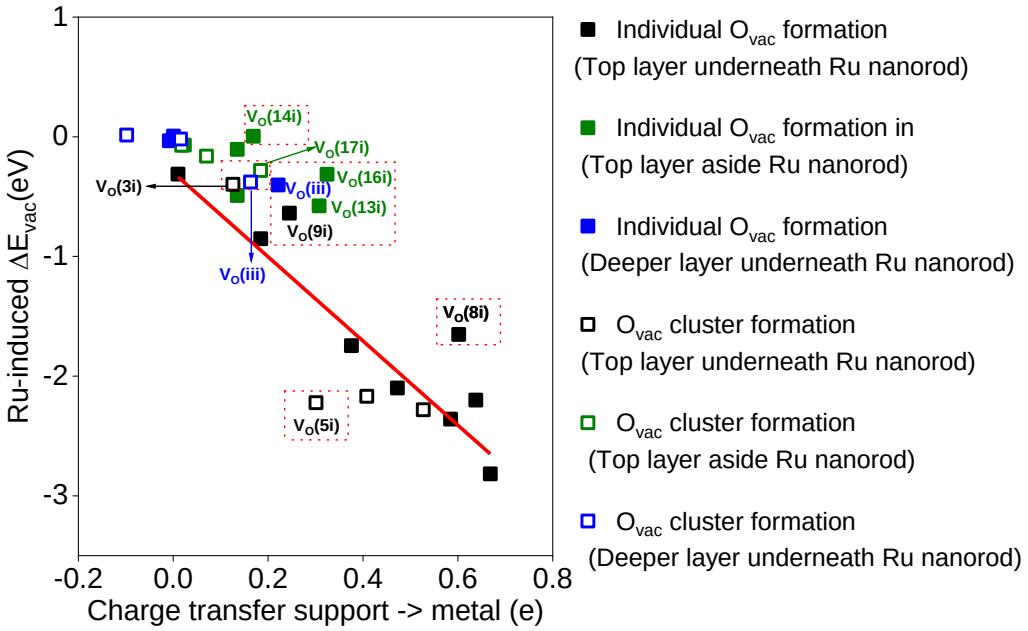

Figure 9. Ru-induced lowering of the O-vacancy formation energy ΔE_{vac} on Ru/ZrO_2 as a function of the charge transfer from the support to the Ru nanorod upon O-vacancy formation, including all configurations discussed so far. Formation of individual O-vacancies on a fully oxidized Ru/ZrO_2 model system is presented as full symbols, O-vacancies as part of a growing O-vacancy cluster on a partly reduced Ru/ZrO_{2-x} system as open symbols. The red line represents the fit to the data in Figure 3c, the data points within the red dashed rectangles have structural contributions ($\Delta E_{Ru}^{deform} + \Delta E_{support}^{deform}$) of 0.29 eV or more.

As a general result, the Ru nanorod can only lead to a significant promotion of O-vacancy formation for oxygen atoms in direct contact with the Ru nanorod (black squares in Figure 9). O-vacancy formation in the surface layer aside the Ru nanorod (green squares in Figure 9) or in deeper layers of the ZrO_2 support underneath the nanorod (blue squares in Figure 9) results in a very small or even negligible lowering of the O-vacancy formation energy as compared to the corresponding O-vacancy formation energy on the bare ZrO_2 support, although there is still some charge transfer possible. Consequently, the related data points are above the red fit line. Furthermore, for O-vacancy formation in O-vacancy islands, in the neighborhood of existing O-vacancies (open symbols), the charge transfer is mostly slightly lower than upon formation

of individual O-vacancies at the same site, which was attributed to depolarization effects, or it is identical. Nevertheless, despite of these deviations, the charge transfer from the support to the Ru nanorod upon O-vacancy formation can be used as a primary indicator for the Ru-induced lowering of the energy cost for creating that O-vacancy. Note that it is not a descriptor, as this would refer to a physical property of the model before formation of the O-vacancy.

3.2. CO adsorption energy

To probe the influence of O-vacancies on the CO adsorption energy, we calculated the CO adsorption energy for different sites of the Ru nanorod, with O-vacancies at the different positions discussed in the previous sections, and both with individual O-vacancies and O-vacancy clusters (sections 3.2.1 – 3.2.3). The resulting trends in adsorption energy are compared with those in various physical parameters such as the charge on the respective Ru adsorption sites or shifts in the center of the local density of d-states on the different Ru surface atoms acting as or contributing to the different adsorption sites, following the established d-band model.[41] Stimulated by the Blyholder model,[42] we also evaluated the change in the charge state of the ZrO_2 support, of the Ru nanorod and of the CO molecule upon CO adsorption, which provides information on the charge transfer to the CO molecule (see Figure 10d). Obviously, this is a considerable simplification of the Blyholder picture, where the charge transfer (donation) from metal d-states into the $2\pi^*$ orbital of the CO molecule in combination with backdonation from the 5σ orbital of the CO molecule into metal states with appropriate symmetry is decisive, as the latter distinguishes between different metal states. It would allow even a considerable strengthening of the metal - CO bond with no net charge transfer, if the contributions from charge donation into the $2\pi^*$ orbital and from the 5σ orbital compensate each other. Nevertheless, it would be interesting to see whether there is a correlation between charge on the Ru adsorption site (before CO adsorption), total charge transfer to the CO and

CO adsorption energy. For adsorption sites involving more than one surface Ru atom, we used the mean value of the d-band centers of the individual Ru surface atoms involved in the bonding. Finally, we performed a similar analysis as described for the O-vacancy formation, splitting the total CO adsorption energy ($E_{ads,Ru/ZrO_{2-x}}$) into contributions from the CO-induced deformation of the Ru nanorod (E_{Ru}^{deform}) and of the support ($E_{ZrO_{2-x}}^{deform}$), from the difference in interface energy in the presence and absence of adsorbed CO ($\Delta E_{Ru-support}^{int}$), and finally the actual CO binding energy on the relaxed adsorption site ($E_{bind,CO}$) according to

$$E_{ads,Ru/ZrO_{2-x}} = E_{Ru}^{deform} + E_{ZrO_{2-x}}^{deform} + \Delta E_{Ru-support}^{int} + E_{bind,CO} \quad (6)$$

The way how these energies are calculated is schematically illustrated in Figure S2.

These data also provide information on the effect of adsorbed CO on the energetics of O-vacancy formation, considering that this can be derived as the difference of the O-vacancy formation energy of a Ru/ZrO_2 model system with an adsorbed CO and the CO_{ad}-free Ru/ZrO_2 model system. Such effects will be briefly discussed in section 3.2.4. Finally, we present an overview on the correlations between the CO adsorption energy on the one hand and the charge on the Ru adsorption site as well as the position of the d-band center on the other hand (section 3.2.5).

In these calculations, we considered CO adsorption on the flat top layer (site Ru-1c in Figure 2b), denoted as 'top layer terrace site', on the edge site at the top layer (sites formed by Ru atoms 7a and 8a in Figure 2b), denoted as 'top layer edge site', on a site in the middle layer at the side of the Ru nanorod (mostly site Ru-5a in Figure 2b), denoted as 'middle layer site', and on two sites at the bottom layer, in the interface region. These two interface sites, which differ by their distances to the ZrO_2 support, are formed either by Ru atoms 1a and 5a or by Ru atoms 2a and 6a in Figure 2b. For adsorption on the 'interface (i)' site, CO may move also to a hollow site formed by Ru atoms 1a, 4a, and 5a, or a bridge site formed by Ru atoms 4a and 5a during

optimization. For adsorption on the 'interface (ii)' site, CO may also move to a hollow site formed by Ru atoms 2a, 3a, and 6a, or to a bridge site formed by Ru atoms 2a and 3a. Furthermore, CO adsorbed on interface (i) and (ii) sites can interact also with the 2Zr and 1Zr cations, respectively. These and other changes in the initial adsorption site are indicated in the following figures by hatched bars for the CO adsorption energy. The energetically preferred adsorption sites on the different systems are listed in Tables S6 and S8, respectively, and also mentioned in the discussion. It should also be noted that in some cases CO was not (meta-) stable on the initial adsorption site and relaxed to another site, e.g., from an interface (i) site to a middle layer site. This would be indicative of a very small or absent energy barrier for CO migration between the two configurations.

3.2.1. Effect of O-vacancies underneath the Ru nanorod on the CO adsorption energy

Effect of individual O-vacancies: To probe the influence of the position of an O-vacancy underneath the Ru nanorod, we first calculated the CO adsorption energy on systems with a single isolated O-vacancy at the interface perimeter, under the edge of Ru nanorod (the 1st and 3rd row of oxygen atoms in Figure 10a) and away from the perimeter sites (the 2nd row oxygen atoms in Figure 10a). While the O-atoms in the 1st and 3rd rows appear symmetric in Figure 10a, their interactions with the Ru nanorod differ due to the mismatch of the Ru nanorod and the support lattices. The most favorable sites for O-vacancy formation, as given by the O-vacancy formation energy (see Figure 3), are the 1i site for the 1st row, the 4i site for the 2nd row, and the 7i site for the 3rd row. Therefore, we calculated the CO adsorption energies on the different adsorption sites ('top layer (terrace)', 'top layer (edge)', 'middle layer', 'interface (i)', and 'interface (ii)' sites) for Ru/ZrO_{2-x} systems with a single O-vacancy at the 1i site (pink bar), at the 4i site (blue bar), and at the 7i site (orange bar), respectively (see Figure 10). For comparison, we also included CO adsorption energies on the fully oxidized Ru/ZrO_2 model system (grey bar), using the same Ru adsorption sites. In our previous work,[21] we had attributed

changes in the CO adsorption energy caused by the introduction of O-vacancies mainly to variations in the charge state of the Ru nanorod, more specifically, of the Ru atoms forming the CO adsorption site, due to electron transfer from the support to the Ru nanorod. Therefore, in the subsequent discussion we are particularly interested in possible correlations between CO adsorption energy and charge state of the Ru atoms contributing to the adsorption site.

The trend in these CO adsorption energies is illustrated in Figure 10b and listed in Table S22. Obviously, the presence of the O-vacancy and the location of the O-vacancy underneath the Ru nanorod have very little influence on the CO adsorption energies on the top layer sites. This follows the trend of the charge variation on the 1c and the 7a / 8a sites for the different O-vacancies, which are also negligible (see Table S30), as expected for an efficient screening by the underlying metal layers. Comparing the CO adsorption energies on the two top-layer sites also shows that adsorption on the edge site is by about 0.25 eV more stable than on the terrace site, which can be understood from the lower Ru coordination at the edge site. The difference is, however, smaller than obtained in earlier calculations for CO adsorption on different metal surfaces, which showed a more pronounced difference of about 0.5 eV for adsorption on Pt terrace and step sites, respectively.[43] This discrepancy may be attributed to the strain on the Ru nanorod induced by the support lattice, which changes the distance between Ru-1c and the neighboring Ru atoms in the terrace area from 2.70 Å to a range between 2.51 and 2.78 Å.

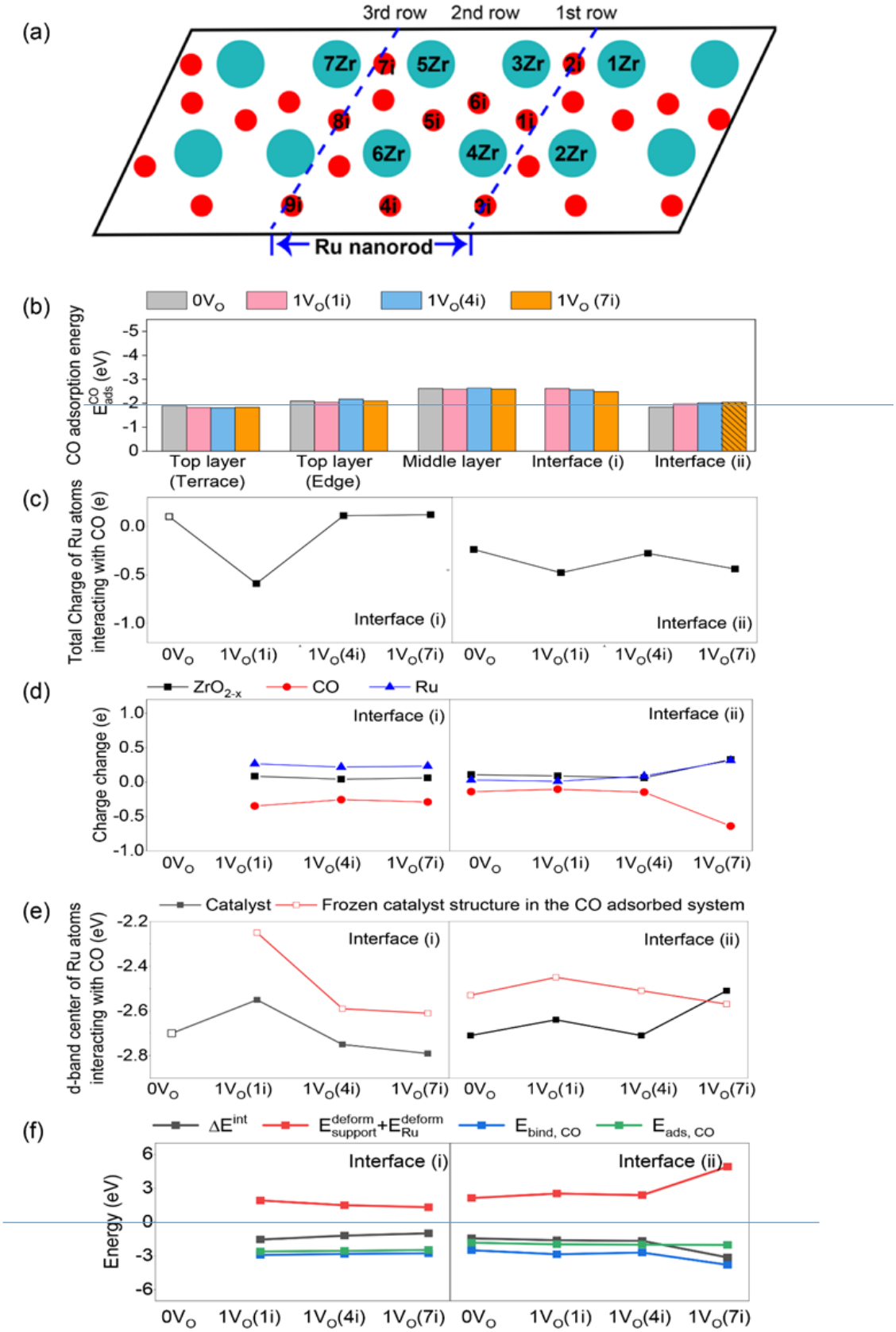

Figure 10. (a) Schematic representation of the support surface layer (top view) and labels of the different Zr surface ions and O-vacancies (see also Figure 2 for comparison).

(b) CO adsorption energies on different Ru sites of the fully oxidized, relaxed Ru/ZrO_2 model system (grey bars) and on the relaxed Ru/ZrO_{2-x} model systems with a single O-vacancy at different positions underneath the Ru nanorod (positions see panel (a)). The dashed bar indicates a change in the CO adsorption site during relaxation (see text). (c) Total charge on the Ru atoms binding to CO on the interface (i) and (ii) sites before CO adsorption. (d) Change in charge state of the support (black squares and line), the Ru nanorod (blue triangles and line) and the CO molecule (red circles and line) upon CO adsorption on interface (i) and (ii) sites. (e) Energy of the d-band center on the Ru surface atoms forming the interface (i) and (ii) sites site relative to the Fermi level for the bare model system (black) and for the system in the frozen structure that would be obtained with CO adsorbed on the respective interface site, but without the CO (red). (f) Different contributions (deformation energies, change in interface energy and CO binding energy, see figure) to the total CO adsorption energy.

Adsorption on the middle layer site is significantly stronger than on the topmost layer, by about 0.4 – 0.6 eV. The presence of an O-vacancy leads to a slight increase in CO adsorption energy compared to the fully oxidized Ru/ZrO_2 system, with little difference for the different O vacancy positions (Figure 10b and Table S22). Since the charge on the middle layer adsorption site (Ru-5a) is essentially identical with that on the top-layer terrace site (Ru-1c), both for the fully oxidized surface and also in the presence of an O-vacancy (Table S30), this larger adsorption energy cannot be simply explained by differences in the charge of the Ru adsorption sites before CO adsorption. We tentatively attribute this stronger bond between the Ru-5a atom and the adsorbed CO to a lower coordination of this Ru surface atom, due to larger bond lengths to some of the neighboring Ru atoms. For the Ru-5a atom, only four Ru neighbors show bond distances of up to 2.70 Å, the Ru-Ru distance in bulk Ru, while for the Ru edge atoms 7a and 8a, six neighboring Ru atoms can be found within this distance. This may shift the d-band center without significant changes in the total charge.[44] Such effects will be discussed in more detail later in this section.

CO adsorption on the interface (i) site is instable on the fully oxidized Ru/ZrO_2 system, in the absence of an O-vacancy. Instead, CO_{ad} will diffuse to the Ru-5a site in the middle layer during relaxation. Since CO changed the type of adsorption site during relaxation, we did not represent its adsorption energy on the interface (i) site in Figure 10b. In fact, after relaxation the CO adsorption site and energy correspond to those on the middle layer site for this system. In the presence of an O-vacancy, CO adsorption becomes stable on the interface (i) site and shows a rather high adsorption energy, comparable to adsorption on the middle layer site, with a subtle decay with increasing distance to the O-vacancy. In this case, the adsorbed CO is also rather close to the Ru-5a atom, though not as close as for adsorption on the middle layer site (Table S10). In the presence of an O-vacancy, CO adsorption on this site is further strengthened by an interaction between the O atom of the CO and the 2Zr surface cation, which is indicated by their rather close distance of about 2.3 Å (Table S10). This CO - Zr interaction decreases with increasing distance of the O-vacancy from the adsorption site (Table S10).

To test for a correlation between the charge on the Ru adsorption site and the CO adsorption energy, we plotted the charge on the Ru atoms interacting with CO (before CO adsorption) in Figure 10c. The charge on the Ru adsorption site (Ru-1a and Ru-5a atoms) is rather low for the fully oxidized system ($0V_O$), which may explain the instability of CO adsorption on the interface (i) site under these conditions. It drastically increases upon formation of the O-vacancy at the 1i site, respectively, and then decreases again for the more distant O-vacancies (see also Table S30). Interestingly, despite the significant modification of the charge on the Ru adsorption site upon O-vacancy formation on the 1i site, this is not reflected by a similarly significant change in the CO adsorption energy, underlining again that the charge on the Ru adsorption site is an important, but not the only factor affecting the CO adsorption energy and /or that the variation in adsorption energy with charge is only small (see also section 3.2.5).

Next, we evaluated the change in the charge state of the ZrO_2 support, of the Ru nanorod and of the CO molecule upon CO adsorption, which provides information on the charge transfer to the CO molecule (see Figure 10d). For adsorption on the interface (i) site, there are only negligible CO adsorption induced changes of the charge on the support, independent of the position of the O-vacancy. For the Ru nanorod, the change is more pronounced, around +0.2 e, independent of the position of the O-vacancy. Accordingly, we find a slightly bigger negative change in electron charge for the adsorbing CO. Also here, the variation is too small to have a sizable impact on the CO adsorption energy. Apparently, the significantly higher charge on the Ru adsorption site on the $1V_O$(1i) system has little effect on the charge transfer to the CO. In combination, these effects lead to rather similar CO adsorption energies on the middle layer and interface (i) sites, which is also independent of the presence of an O-vacancy and its position.

CO adsorption on the interface (ii) site is less stable than on the interface (i) site, more comparable to that on the top layer sites. In the presence of an O-vacancy, we find a subtle increase of the CO adsorption energy, which remains about constant with increasing distance of the O-vacancy from the adsorption site, from -1.84 eV (fully oxidized) to -1.98 − -2.05 eV. In this case, there is some variation in the charge on the Ru atoms interacting with CO upon varying the O-vacancy position (Figure 10c), but this seems to be too small to significantly affect the trend in the CO adsorption energy. Note that the increase in electron charge on the Ru adsorption site when going to the $1V_O$(7i) system is mainly due to a change in Ru adsorption site, from Ru-2a/Ru-6a to a Ru-2a/Ru-3a bridge site, while the charges on the different Ru surface atoms remain almost constant. Finally, the data in Figure 10d indicate that the changes of the charge on the support, the Ru nanorod and CO upon CO adsorption are generally small, significantly less than for CO adsorption on the interface (i) site. Hence, the net charge transfer to the CO, into the $2\pi^*$ orbital and from the 5σ orbital of CO, is much less. Only for the $1V_O$(7i)

system, there is a stronger increase in charge transfer to the CO molecule for this system, similar to the increase in charge on the Ru adsorption site in this case. Most simply, this is due to the change in adsorption site, with its higher total charge. However, this does not seem to have a significant impact on the CO adsorption energy on this site, which is comparable to that on the $1V_O$(4i) system.

The energies of the d-band centers on the individual Ru surface atoms are tabulated in Table S47. The resulting energies obtained for the interface sites are illustrated in Figure 10e. In perfect agreement with the trend in the CO adsorption energy, there is essentially no change in the d-band center on the Ru-5a atom (middle layer site) (Table S47). For the interface (i) site, the bridge site with the Ru-1a and Ru-5a atoms is rather unfavorable due to the low d-band center of the Ru-1a atom (-2.95 eV), which is in good agreement with the spontaneous shift of CO adsorbed on the interface (i) site to the middle layer site. Formation of an O-vacancy on the 1i site, directly underneath the edge of the Ru nanorod (Figure 10a), results in a significant upshift of the d-band center (Figure 10e), which goes along with stable adsorption on this site. For O-vacancies located further away from the edge of the Ru nanorod and hence from the interface (i) site, the d-band center decreases again, in good agreement with the slight decrease of the CO adsorption energy (Figure 10b).

In general, the d-band model relates the CO adsorption energy to the energy of the d-band center of the respective surface atom on the bare metal, in the absence of an adsorbate [41]. Considering that adsorption can go along with a more or less pronounced restructuring of the metal, it would appear more plausible to use the d-band center of the restructured metal as reference. Therefore, we performed similar calculations for the Ru/ZrO_2 systems with the structure frozen to that of the system carrying an adsorbed CO atom, but without the CO atom. This also means that the LDOS and thus the d-band centers on the respective Ru surface atoms may vary for different CO adsorption sites and hence slightly different Ru nanorod structures. Such effects are

expected to be minor for adsorption on single-crystalline low-index metal surfaces, where adsorbate induced structural modifications are mostly small, while on structures like the present nanorod structures they may be more significant. The d-band centers resulting for the frozen structures of the Ru/ZrO_x systems with a CO molecule on the top layer edge site or on the middle-layer site are compiled in Tables S48 and 49, respectively. They exhibit slightly more pronounced, but still small changes, in the range of ±0.1 eV, which is comparable to the trend in the CO adsorption energy. Hence, structural effects seem to be negligible in this case. For the systems frozen into the structure obtained for CO adsorbed on the interface (i) site, but with the CO_{ad} removed, the resulting d-band center energies plotted as red line in Figure 10e and listed in Table S50. These data show a similar trend upon O-vacancy formation as obtained for the original system (black line), but with the d-band center about 0.2 eV higher. Hence, the CO_{ad} induced structural deformation leads to an enhanced ability to interact with CO (formation of the adsorption bond), while the trend for different O-vacancy locations does not change.

Similar calculations were performed for CO adsorption on the interface (ii) site. For the original structure of the model system, we obtain the trend in the d-band center illustrated in Figure 10e, right panel. For the first three systems, there is little difference compared to the d-band center energies of the interface (i) site, while there are considerable differences in the CO adsorption energies on these sites. A possible reason for this discrepancy will be discussed below in this section. Second, there are only small changes in the d-band center for O-vacancies at the 1i and the more distant 4i site compared to the fully oxidized state, which also agrees well with the trend in the CO adsorption energy. For the O-vacancy on the 7i site, the d-band center suddenly up-shifts. This shift is mainly caused by the change in the Ru adsorption site, from Ru-2a / Ru-6a to Ru-2a / Ru-3a (Table S51), since for this O-vacancy position the d-band center on the Ru-3a atom shows a pronounced upshift, while on the Ru-5a atom it down-shifts by 0.3 eV. These counteracting shifts provide a clear driving force for the spontaneous change in adsorption site

during relaxation (see Table S6). This trend fits also to the enhanced charge transfer to the CO for this system (Figure 10d), while the CO adsorption energy increases only little. Finally, for the d-band center on the frozen structure (red line in Figure 10e right, see explanation above), the values follow the trend obtained for the original structure of the Ru nanorod (black line in Figure 10e, right), only up-shifted by about 0.2 eV. Similar to adsorption on the interface (i) site, CO_{ad} induced restructuring increases the ability to form a strong CO adsorption bond. Only for the last system, with an O-vacancy on the 7i site, the d-band center energy does not follow the trend obtained for the original structure, but rather exhibits a slight further down-shift. The much smaller change from the $1V_O$(4i) system to the $1V_O$(7i) system seems to fit better to the small change in CO adsorption energy than the bigger change obtained for the original structure, although we consider changes in the d-band center of >0.2 eV to be at the limit of the predictive power of the d-band model.

Finally, analysis of the different contributions to the total CO adsorption energy ($E_{ads,Ru/ZrO_{2-x}}$) on the interface (i) site revealed that the O-vacancy on the 1i site results in a slightly higher negative contribution from the change in interface energy upon CO adsorption ($\Delta E^{int}_{Ru-support}$) than obtained for the O-vacancies on 4i and 7i sites, which are further away from the adsorption site (Figure 10f and Table S24). This, however, is compensated by a slightly higher positive contribution from the deformation energies, leaving the total CO adsorption energy essentially constant. For adsorption on the interface (ii) site (Figure 10f and Table S25), the difference between CO binding energy and CO adsorption energy, which is given by the sum of the CO_{ad} induced deformation energy and difference in interface energies, is generally bigger than for adsorption on the interface (i) site. Apparently, these latter contributions are mainly responsible for the lower adsorption energies on the interface (ii) site. This is particularly true for adsorption on this site in the $1V_O$(7i) system

In total, the effect of the O-vacancies on the CO adsorption strength is rather small in these cases, less than 0.2 eV at most, which is significantly less than the difference in adsorption energy between adsorption on top layer or interface (ii) sites on the one hand and middle layer or interface (i) sites on the other hand. Furthermore, the CO adsorption energy does not vary much with the position of the vacancy underneath the Ru nanorod. The general difference between adsorption on the different interface sites seems to mainly result from the differences in the (positive) contributions from the sum of the CO_{ad} induced deformation energies and changes in the interface energies between these sites, which are more pronounced for adsorption on the interface (ii) site than for adsorption on the interface (i) site, leading to lower adsorption energies on the interface (ii) sites. The remaining small changes in the CO adsorption energy for different positions of the O-vacancies seem to largely follow the trend given by the charge on the respective Ru adsorption sites and by the position of the d-band center. For adsorption on the top layer and middle layer sites, the small O-vacancy induced changes in the charge state or the CO adsorption energy reflect an effective metallic screening of the transferred charge. The higher adsorption energy on the middle layer site and on the interface site (i) site compared to the adsorption on the top layer sites is mainly attributed to coordination effects, which are reflected also in the up-shifted captured energies of the d-band center (see Table S47). This effect is present also for adsorption on the interface (ii) site, but counteracted and compensated by the higher positive contribution from the deformation energy and change in interface energy. Finally, for adsorption on the interface sites, direct interactions between the O atom of CO and a Zr surface ion aside an O-vacancy with distances around 2.3 Å may play a role as well in some cases.

Effect of O-vacancy clusters: Due to the more pronounced total charge transfer to the Ru nanorod, the presence of an O-vacancy cluster directly underneath the Ru nanorod may lead to stronger effects in CO adsorption than the single O-vacancies discussed so far. Following the

procedure in section 3.1.1, we started by removing the surface oxygen atom from site 1i, followed by removal from the 2i and 3i sites, forming the $1V_O$, $2V_O$, and $3V_O$ clusters. Subsequent removal of the more central O atoms at the 4i and 5i sites leads to the $5V_O$ cluster. It should be noted that this cluster does not include O-vacancies in the 3rd row such as site 7i. The CO adsorption energies, calculated for the same CO adsorption sites as described above, are presented in Figure 11a. For comparison, we also included CO adsorption energies on the fully oxidized Ru/ZrO_2 system (grey bars), which were already shown in Figure 10b.

Similar to the results obtained for individual O-vacancies at different locations, also the effect of growing O-vacancy clusters underneath the Ru nanorod and thus with increasing charge on the Ru nanorod (see Table S31) on the adsorption energy (see Table S23) is generally rather small for CO adsorption on the topmost layer and on the middle layer site ($\Delta E_{ad} \leq 0.25$ eV). This can again be explained by an efficient metallic screening. In contrast, there are significant changes in the CO adsorption energy for adsorption at the interface sites. For adsorption on the interface (i) site, where CO adsorption is not stable on the fully oxidized system, but stabilized by an O-vacancy on the 1i site (Figure 11a), we find little variation up to the $3V_O$ system, but a distinct decrease of the CO adsorption energy for the $5V_O$ system. Possible reasons for that will be discussed in more detail below.

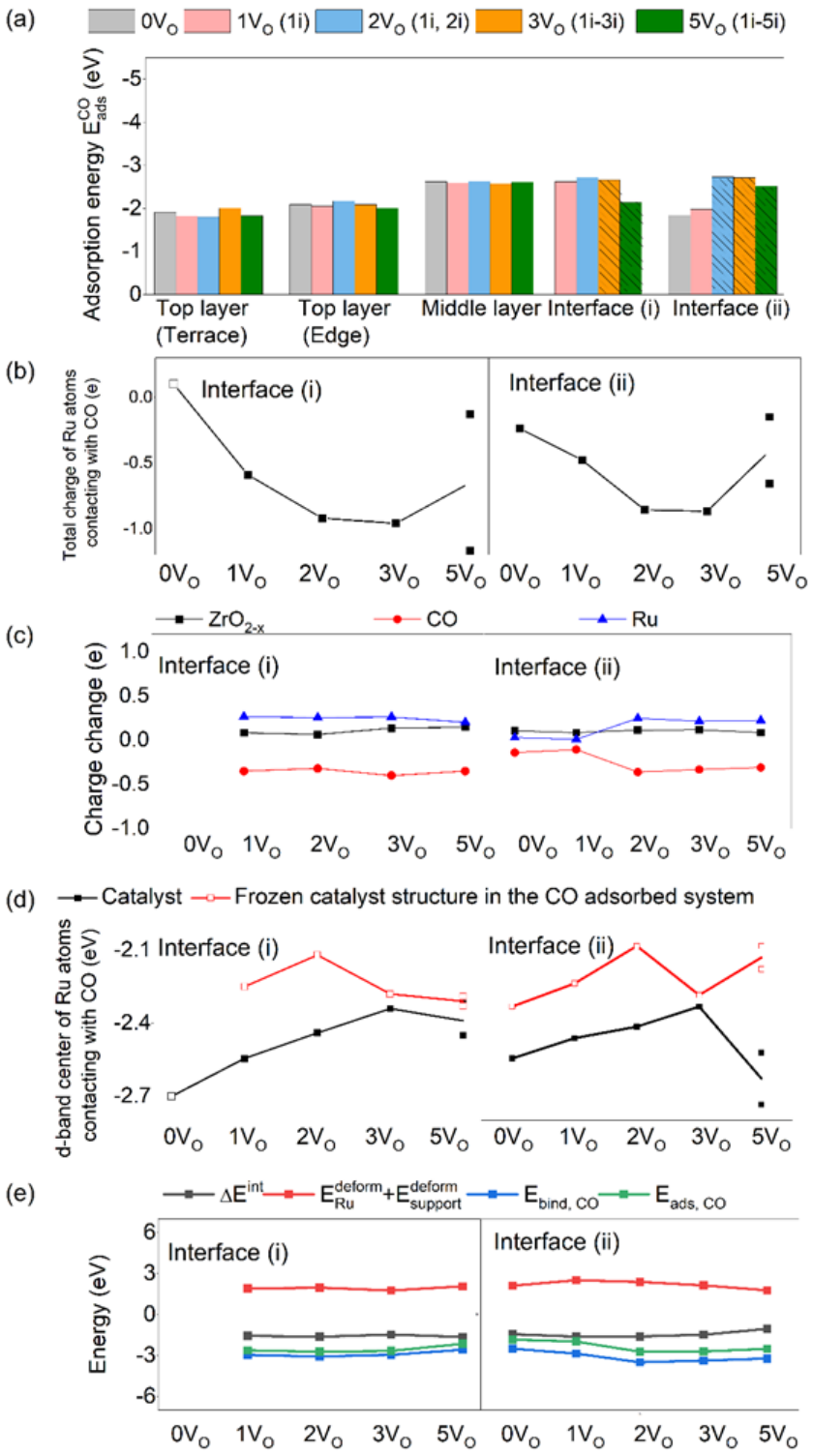

Figure 11. (a) CO adsorption energies on different sites on the fully oxidized, relaxed Ru/ZrO_2 (grey bar) and on the partly reduced, relaxed Ru/ZrO_{2-x} model systems with different O-vacancy clusters underneath the Ru nanorod ($1V_O$: pink bar, $2V_O$: blue bar, $3V_O$: orange bar, and $5V_O$: green bar). (b) Total charge on the Ru atoms binding to CO on the interface (i) and (ii) sites before CO adsorption. (c) Change in charge

state of the support (black squares and line), the Ru nanorod (blue triangles and line) and the CO molecule (red circles and line) upon CO adsorption on interface (i) and (ii) sites. (d) Energy of the d-band center on the Ru surface atoms forming the interface (i) and (ii) sites site relative to the Fermi level for the bare model system (black) and for the system in the frozen structure that would be obtained with CO adsorbed on the respective interface site, but without the CO (red). (e) Contributions from CO_{ad} induced deformation energies, change in interface energy and CO binding energy (see figure) to the total CO adsorption energy.

Figure 11b illustrates the total charge of the Ru atoms binding to CO at the interface sites. For adsorption on the interface (i) site (Ru-1a, Ru-5a, 2Zr) of the fully oxidized Ru/ZrO_2 system, where CO adsorption is not stable, the charge on this site would be rather small, around 0.1 e (Table S31), which may provide a simple explanation for the spontaneous shift of CO_{ad} from this site to the middle layer site (Ru-5a) during relaxation. In the presence of one or two O-vacancies, this charge increases from -0.59 e ($1V_O$) to -0.92 e ($2V_O$), which is mostly due to a pronounced charge increase on the Ru-1a atom in the bottom layer, from -0.62 e ($1V_O$) to -1.02 e ($2V_O$) (Table S31). For the $3V_O$ system, CO_{ad} moves to the threefold hollow site formed by the Ru-1a, Ru-4a and Ru-5a atoms (Table S8). Because of the little charge on the Ru-4a atom and the small charge changes on the other two Ru atoms (Table S31), formation of the third O-vacancy ($3V_O$) has little effect on the charge on the adsorption site (-0.96 e). Finally, upon formation of the fourth and fifth vacancy, for the $5V_O$ system, the charge on the Ru adsorption site decreased abruptly to -0.13 e. Also this is mainly due to a change in the Ru adsorption site, since the more strongly charged Ru-1a atom, with its significantly enhanced Ru-1a - C(CO) bond distance (2.29 Å, Table S13) is not considered as part of the adsorption site in the most stable configuration any more. On the other hand, however, based on the distance between Ru-1a and CO, there still seems to be some interaction between CO and the Ru-1a atom in the $5V_O$ system. Therefore, we additionally plotted a data point which includes also the charge on the Ru-1a atom for comparison. Assuming that the real situation will be somewhere between the

two data points for the $5V_O$ system, there is some decrease in the charge state, by about 0.3 e to lower charge, which brings it back to the value obtained for the $1V_O$ system. Considering this, the change in charge state from $3V_O$ to $5V_O$ seems to be much less than the change in CO adsorption energy. Finally, it is interesting to note that this decay in adsorption energy is not reflected by a change in electron charge on the support, Ru nanorod or CO upon CO adsorption (Figure 11c, left). We will get back to this open question when discussing the shifts in the energy of the d-band center further below.

For CO adsorption on the interface (ii) site, adsorption on the fully oxidized Ru/ZrO_2 and on the $1V_O$ system are comparable in strength to adsorption on the top layer terrace site. Here, we find an increase in charge, mostly on the Ru-2a atom, already when moving from the $0V_O$ to the $1V_O$ system (Figure 11b), while the bridge adsorption site (Ru-2a and Ru-6a) is maintained. This charge increase goes along with a small increase in the CO adsorption energy (Figure 11a). The rather low adsorption energy fits well also to the rather low charge transfer from the Ru to the CO for adsorption on the $0V_O$ and $1V_O$ systems (Figure 11c).

Moving on to the $2V_O$ system, we find a pronounced increase of the charge on the Ru-3a surface atom (Table S31), which leads to a change in the adsorption site to the (Ru-2a, Ru-3a, Ru-6a) threefold hollow site. Hence, for the $2V_O$ system, adsorption on this site is more stable than on the Ru-2a / Ru-6a bridge site, while for the $0V_O$ and $1V_O$ systems it was opposite. This goes along with a pronounced increase in CO adsorption energy on the $2V_O$ system (Figure 11a). Furthermore, the change in adsorption site causes a further steep increase of the charge on the adsorption site, which is mainly due to the additional contribution of the Ru-3a atom (Table S31). This also leads to an increased charge transfer from the Ru nanorod to the adsorbed CO. With further increasing O-vacancy cluster size, the CO adsorption energy decreases slightly, but the decay is much less than that observed for adsorption on the interface (i) site when going to the $5V_O$ system. For the $3V_O$ system, this goes along with an essentially constant total charge

on the Ru adsorption site and a slightly smaller electron transfer to the CO molecule upon CO adsorption. Finally, when moving from the $3V_O$ to the $5V_O$ system, we find a significant decrease in charge on the Ru adsorption site, mainly on the Ru-2a atom (Table S31), while there is only a minor decay in the charge transfer to the adsorbing CO, and also the decay in CO adsorption energy is less pronounced than observed for the interface (i) site at this point (Figure 11a and 11c). Also this will be dealt with further when discussing the related shift in the d-band center.

In total, these results support a picture in which the CO adsorption strength is mainly determined by the charge transfer from the Ru nanorod to the adsorbed CO molecule upon adsorption, which in turn is mainly determined by the charge on the Ru atoms serving as adsorption site. Hence, a decreasing electron density at the adsorption site disfavors electron transfer from the Ru adsorption site atoms to the adsorbed CO molecule. Considering also that the charge transfer from the support to the Ru nanorod upon O-vacancy formation is highly local, CO adsorption is mainly affected by O-vacancies formed close to the adsorption site. Additional surface O-vacancies further away from the Ru atoms at the interface perimeter have less or very little effect on the CO adsorption energy at these Ru atoms, due to metallic screening. For the same reason, due to the localization of charge transfer to the interface Ru atoms, CO adsorption in higher layers is hardly affected by the formation of O-vacancies underneath the Ru nanorod.

Similar to the evaluation of the role of individual O-vacancies, we calculated the local density of states (LDOS) on the Ru surface atoms contributing to the respective middle layer and interface adsorption site and the resulting energies for the center of the d-band. As before, there is essentially no change in the d-band center on the Ru-5a atom (middle layer site) (Table S52), in full agreement with the trend in the CO adsorption energy. For the interface (i) site, we obtain a continuous increase of the d-band center up to the $3V_O$ system (black line in Figure 11d, left), in qualitative agreement with the trend in the CO adsorption energy (Figure 11a). For the $5V_O$

system, this trend would continue if we only consider the Ru-4a and Ru-5a atoms for the adsorption site, which would be opposite to the trend in the adsorption energy. When including, however, also the Ru-1a atom, which in this case is still rather close to the CO (Table S13), the d-band center decreases slightly (see Figure 11d and Table S52), though less pronounced than the decay of the (calculated) CO adsorption energy. For the interface (ii) site, similar calculations result in the trend of the d-band center illustrated in Figure 11d, right (see also Table S52). Also in this case the trend of the d-band center does not fully reproduce that of the CO adsorption energies with their distinct increase for the $2V_O$ and larger O vacancy clusters. We assume that this is mainly due to an increased interaction between CO and the 1Zr surface cation, as reflected by the sudden drop in their bond distance (Table S13). Obviously, such effects cannot be captured by the d-band model.

Next, we explored the effects of restructuring. The d-band centers resulting for the frozen structures of the Ru/ZrO_x systems with a CO molecule on the top layer edge site or on the middle-layer site are compiled in Tables S53 and S54. The changes in the d-band center on the Ru-5a atom (middle layer adsorption site) are slightly more pronounced than on the original system, but still small, in the range of ±0.1 eV, and thus comparable to the trend in the CO adsorption energy. Hence, in this case structural effects seem to be negligible.

For the systems frozen into the structure obtained for CO adsorbed on the interface (i) site, but with the CO_{ad} removed, the resulting d-band center energies are listed in Table S55. Similar to our findings for the individual O-vacancies, the d-band centers follow the trend obtained for the original structure up to the $2V_O$ system (two O-vacancies), but shifted upwards by about 0.2 eV (red line in Figure 11d). Hence, also in this case, CO_{ad} induced restructuring stabilizes the Ru – CO interaction. Going to the $3V_O$ system, the d-band center down-shifts significantly, different from the further up-shift obtained without structural modification (black line in Fig. 11d). In this case, the structural modification would be expected to weaken the CO adsorption

energy compared to that on the $2V_O$ system. The calculated CO adsorption energy indeed decreases from the $2V_O$ to the $3V_O$ system, but the change is very small (Figure 11a). Finally, for the $5V_O$ system, the d-band center remains about constant, while the CO adsorption energy decreases significantly (Figure 11a). Considering that also the interaction between CO and the 2Zr surface ion changes very little, as indicated by the about constant distance (Table S13), this illustrates the limits of a quantitative correlation between d-band center energy, in particular on more complex systems. Comparison with the trends in the different contributions to the CO adsorption energy does (Figure 11e) shows negligible changes in the deformation and interface energies when going from the $1V_O$ to the $3V_O$ system, which remain also for the $5V_O$ system, leaving the CO adsorption energy almost constant. Apparently, this change in deformation and interface energy is related to a CO_{ad} induced re-positioning of the Ru-4a atom by about 0.5 A (Δd_{Ru}^{max} in Table S27), as a consequence of a strong interaction between CO_{ad} and the Ru-4a atom, which is responsible also for the change in adsorption site from Ru-1a/Ru-5a to the Ru1a/Ru-4a/Ru-5a site. Addition of two more O vacancies in the $5V_O$ system causes a decrease of the CO binding energy, which is lower than in other cases. Together with the positive contributions (about 0.4 eV) from the deformation energies plus the difference in interaction energies, this leads to a significant lowering of the CO adsorption energy (Figure 11a and Table S27).

Also for the interface (ii) site we find a similar trend for the restructured Ru nanorod as for the original structure up to the $2V_O$ system, with a continuous up-shift of the d-band (see Figure 11d, right and Table S56). Like for the interface (i) site, re-structuring up-shifts the d-band center by about 0.2 eV compared to the systems in the original structure. Comparing with the CO adsorption energy, the continuous slight increase from $0V_O$ to $1V_O$, followed by a significant increase to the $2V_O$ system, is at best qualitatively reproduced by the more continuous shift of the d-band center. Going to the 3V and $5V_O$ systems, we find distinct differences in the trend of the d-band center between restructured and non-restructured systems.

While for the non-restructured systems it first continues to up-shift and then down-shifts again, the trend is opposite for the restructured systems. For comparison, the CO adsorption energy remains almost constant when going to the $3V_O$ system and decreases when going to the $5V_O$ system. Since also the interaction between CO and the 1Zr cation does not change (Table S13), the question for the physical origin of the pronounced decay in CO adsorption energy in the $5V_O$ system must remain open. Most likely, these changes are too small to be reproduced by the more qualitative nature of the d-band model. In this case, the trend in the CO adsorption energy mostly follows that in the CO binding energies, while changes in the deformation energies and in the interface energies seem to largely compensate each other.

Finally, analysis of the different contributions to the total CO adsorption energy ($E_{ads,Ru/ZrO_{2-x}}$) revealed distinct changes in the interface and deformation energies for adsorption on the interface (i) site when going from the $2V_O$ to the $3V_O$ system. These changes, however, seem to cancel each other, leading to an essentially constant CO adsorption energy. Upon addition of two additional O-vacancies ($5V_O$ system), these contributions slightly change into the opposite direction. In this case, however, they do not fully cancel, which in combination with a slight lowering of the CO binding energy results in the lower CO adsorption energy illustrated also in Figure 11a.

For adsorption on the interface (ii) site, the changes are more subtle. In this case, the CO adsorption energy follows the trend in the CO binding energy, while changes in the other two contributions, from restructuring and changes in the interface energy, largely cancel out. This change in CO adsorption energy is most pronounced when going from the $2V_O$ to the $3V_O$ system, similar to the increase in CO binding energy at this point. Similar to our observation for individual vacancies, the differences between CO binding energy and CO adsorption energy are bigger for adsorption on the interface (ii) site (Table S25) than for adsorption on the interface (i) site (Table S24), indicating that also in this case the lower CO adsorption energies

on the interface (ii) site are mainly due to larger (positive) contributions from the CO_{ad} induced deformation energies and differences in the interface energies.

In total, these results indicate that also for O-vacancy clusters the changes in CO adsorption energy with increasing cluster size are generally small, ≤ 0.2 eV, when not considering the cases where additional direct CO - Zr interactions result in large changes of the adsorption energy. This is again significantly less than the difference between CO adsorption on top layer and interface (ii) sites on the one hand and middle layer sites and interface (i) sites on the other hand. The lower CO adsorption energies on the interface (ii) sites compared to interface (i) sites are again mainly due to larger combined (positive) contributions from CO_{ad} induced deformation energies and changes in interface energies. Apart from these effects, the trend in CO adsorption energy follows at least qualitatively the trends in the charge and in the d-band center on the respective adsorption sites CO before adsorption. Finally, interactions between CO and partly reduced Zr surface ions adjacent to O-vacancies, can significantly increase the CO adsorption energy. Such interactions, which are indicated by close distances between CO and the respective Zr surface ion, are not captured by the d-band model, and the same is true also for CO_{ad} induced deformation energies and changes in the interface energies. Nevertheless, when focusing on a specific adsorption site, the correlation between CO adsorption and charge / energy of the d-band center on the adsorption site works rather well (see also section 3.2.5), underlining the potential of using the charge or d-band center position before CO adsorption as descriptor for the CO adsorption energy also in such complex systems as the present ones.

3.2.2. Effect of O-vacancies aside the Ru nanorod on the CO adsorption energy

In a similar way, we evaluated changes in the CO adsorption energy on the different sites induced by the presence of O-vacancies aside the Ru nanorod, without direct contact to it (see section 3.1.2). Here we tested the influence of O-vacancies at sites 16i, 18i and 13i, which

because of their different distances to the closest Ru atom of ~4 Å, ~6 Å and ~7.3 Å (see Figure 5a) can be considered as representative for the sites in the first row (sites 16i, 18i) and second row (13i-15i) (Figure 12a). The CO adsorption energies resulting for adsorption on the fully oxidized Ru/ZrO_2 system (grey bars) and for adsorption on the Ru/ZrO_{2-x} systems with a single O-vacancy are displayed in Figure 12b. Similar to the results for individual O-vacancies underneath the Ru nanorod (Figure 10b), we find essentially no changes for CO adsorption on the top layer. For adsorption at the middle layer site, which is generally slightly stronger again than on the top layer sites, CO is mostly adsorbed on the Ru-5a atom. Only for the system with the O-vacancy at the 16i site it spontaneously migrates to the hollow site formed by the Ru-1a, Ru-2a, and Ru-5a atoms (Table S6) (hatched bar in Figure 12b). This site is identical with the interface (i) adsorption site. The about constant CO adsorption energy on the fully oxidized system and for O-vacancies on the 18i and 13i sites agrees fully with the essentially constant charge on the Ru adsorption site (Ru-5a atom) (Table S34). For the O-vacancy at the 16i site, where the charge on the Ru adsorption site, in particular on the Ru-2a atom, is considerably more negative (Figure 12c), the CO adsorption energy is significantly higher, as would be expected if there is a correlation between Ru charge state and CO adsorption energy. In this case, CO interacts also directly with the support, in particular with the partly reduced 2Zr ion adjacent to the O-vacancy, and the electron transfer from the support to the CO molecule further strengthens the interaction between CO and the model catalyst (see Figure 12d and Tables S34 and 35). This is reflected also by the decrease of the distance between the 2Zr ion and the O atom of the CO molecule, from 2.52 Å for the fully oxidized system to 2.17 Å for the vacancy at the 16i site (13i: 2.37 Å, 18i: 2.40 Å) (Table S11). For the other systems, this charge transfer is less pronounced. The stronger CO adsorption energy results mainly from an increase of the CO binding energy, while contributions from the deformation and interface energies largely cancel out (Figure 12e).

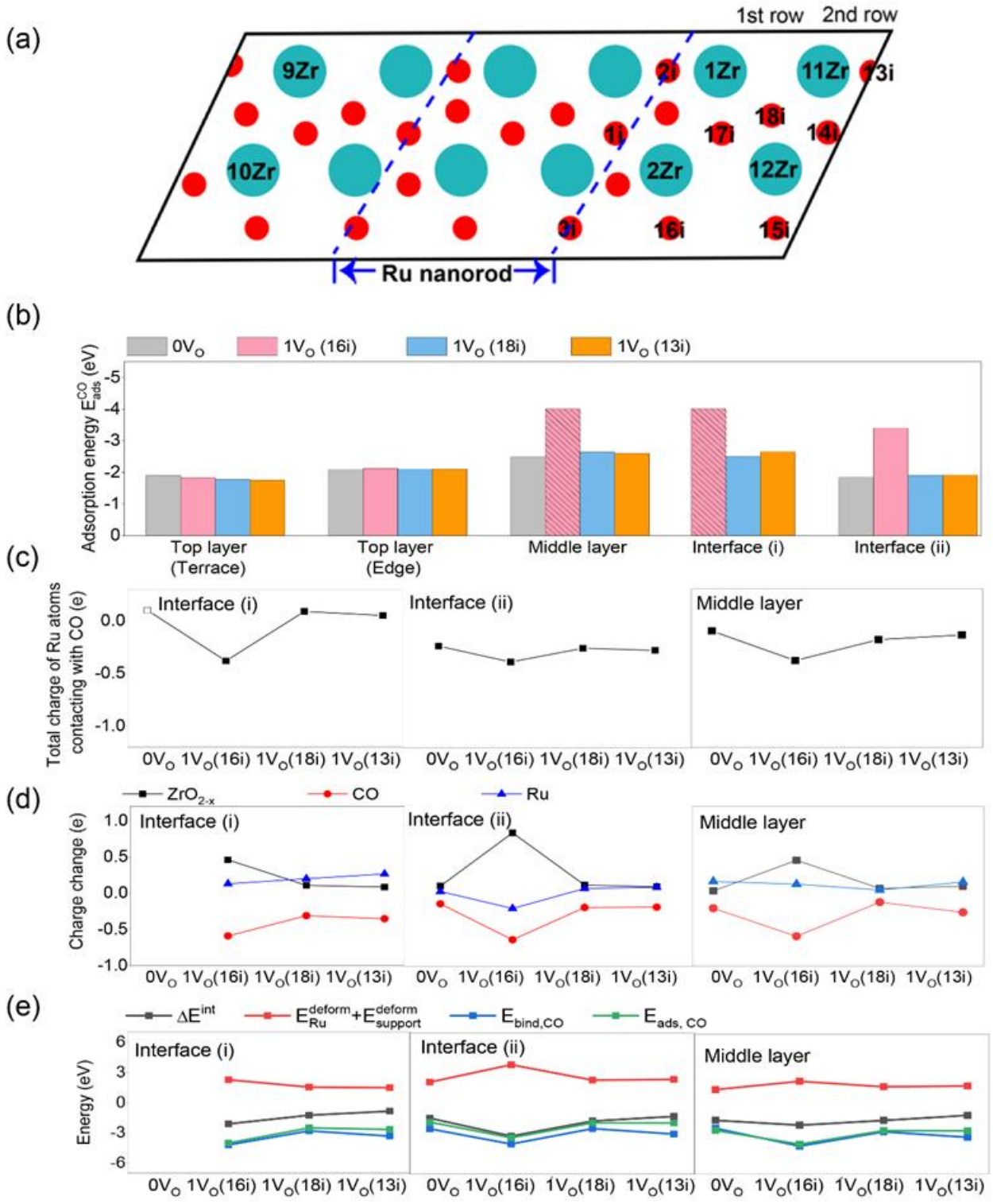

Figure 12 (a) Schematic representation of the surface and indication of the different Zr surface ions and O-vacancies (see also Figure 2 for comparison). (b) CO adsorption energy on different sites of the relaxed Ru/ZrO_2 (grey bar) and the partly reduced, relaxed Ru/ZrO_{2-x} model system with a single O-vacancy at 16i (pink bar), 18i (blue bar), and 13i (orange bar). (c) Charge state of the Ru adsorption sites (middle layer site, interface (i) site, interface (ii) site) on these model systems before CO adsorption.

(d) Change in charge state of the support (black squares and line), the Ru nanorod (blue triangles and line) and the CO molecule (red circles and line) upon CO adsorption on interface (i) and (ii) sites. e) Contributions from CO_{ad} induced deformation energies, change in interface energy and CO binding energy (see figure) to the total CO adsorption energy.

Similar trends are observed for CO adsorption on the interface (i) site (Ru-1a, Ru-5a). As discussed before, CO adsorption on this site is not stable on the fully oxidized Ru/ZrO_2, therefore there is no bar for this case in Figure 12b. Furthermore, similar to adsorption on the middle layer site, CO tends to spontaneously diffuse to the hollow site formed by the Ru-1a, Ru-2a, and Ru-5a atoms for the O-vacancy at the 16i site (Table S6). This results in a significantly higher CO adsorption energy, identical to that obtained for adsorption on the middle layer site for this system (hatched bar in Figure 12b). Again, the stronger bond with CO is partly due to the interaction of CO with the partly reduced 2Zr ion adjacent to the O-vacancy, and the direct electron transfer from the partly reduced Zr ion to the CO molecule (see Figure 12d and Tables S34 and S36). In this case, the distance between the 2Zr ion and the O atom of the CO molecule, decreases from 2.52 Å on the fully oxidized system to 2.17 Å in the presence of a vacancy at the 16i site (Table S11). In the presence of O-vacancies on the more distant 18i or 13i sites, changes in the physical properties of the adsorption site are little, in agreement with the trend in the CO adsorption energy.

For CO adsorption at the interface (ii) site (Ru-2a, Ru-6a), the CO adsorption energy is generally smaller than for adsorption at the middle layer and the interface (i) sites and more comparable to adsorption on the top layer sites. Similar as in the case of O-vacancies directly underneath the Ru nanorod (section 3.2.1), we attribute this mainly to larger positive contributions from CO_{ad} induced deformation energies and differences in the interface energies, which result in a lower CO adsorption energy. This is reflected also by the larger difference between CO binding energy and CO adsorption energy for adsorption on the interface (ii) site

as compared to adsorption on the interface (i) site. Only for the O-vacancy at the 16i site, CO adsorption at the interface (ii) site results in a significant charge transfer from the support to the adsorbing CO, while for O-vacancies at the other two sites the transfer is less, in agreement with the lower adsorption energies on those systems (Figure 12d). Interestingly, this charge transfer upon CO adsorption stems from both the 1Zr and the 2Zr ion, as indicated by their re-oxidation upon CO adsorption (Tables S34 and S37). The stronger interaction with the support is reflected also by the distance between the 2Zr ion and the O atom of the CO molecule, which decreases from 3.29 Å for the fully oxidized system to 2.29 Å for the O-vacancy at the 16i site and then returns again to 2.94 Å for the O-vacancy at the 18i site (Table S11). The distance to the 1Zr ion of about 4.80 Å, in contrast, is significantly larger, making a direct charge transfer hardly likely. This stronger interaction with the support goes along with a more positive deformation energy, which, however, is largely compensated by a comparable increase of the (negative) change in interface energy. Thus, also in this case the increase in CO adsorption energy is mostly due to a similar increase in CO binding energy.

In total, except for the contributions arising from CO interaction with the partly reduced Zr surface ions and the resulting charge transfer from the support to the CO, the presence of O-vacancies further away from the Ru nanorod hardly affects the CO adsorption energy. For the other contributions to the CO adsorption energy, the sum of the CO induced deformation energies and the direct interactions between CO and partly reduced Zr surface ions neighbored to O-vacancies, we refer to our discussion in the previous section 3.2.1. The only difference is that in this case the abrupt increase of the CO adsorption energy due to direct interaction of CO with the partly reduced Zr surface ions neighbored to the O-vacancy on the 16i site is much more pronounced than observed for O-vacancies underneath the Ru nanorod (section 3.2.1). Such interaction is observed for adsorption on both interface sites and also for adsorption on the middle layer site.

Effect of O-vacancy clusters: As in section 3.2.1, we also evaluated the CO adsorption energies at similar or comparable sites in the presence of O-vacancies in vacancy clusters aside the Ru nanorod, starting from a vacancy on site 1i in the $1V_O$ system and proceeding to site 17i in the $2V_O$ system, site 18i in the $3V_O$ system, and finally to site 14i in the $4V_O$ system. These sites were chosen because they are adjacent to each other, with an increasing distance from the Ru nanorod. Figure 13a illustrates the CO adsorption energies at the aforementioned sites in the $1V_O$, $2V_O$, $3V_O$, and $4V_O$ systems, along with the fully oxidized Ru/ZrO_2 system denoted as $0V_O$. Note that during optimization, CO adsorbed at the edge site of the top layer systems shifts to the hollow site formed by the Ru-7a, Ru-8a, and Ru-5a atoms in the $2V_O$ and $3V_O$ systems (Table S8). Similarly, upon adsorption at the interface (i) site (Ru-1a, Ru-5a), CO relaxes to the threefold hollow site formed by the Ru-1a, Ru-4a and Ru-5a atoms for the $3V_O$ and $4V_O$ systems. A comparable shift is observed also for CO adsorption at the interface (ii) site (Ru-2a, Ru-6a), where CO relaxes to the bridge site formed by the Ru-2a and Ru-4a atoms in the $2V_O$, $3V_O$, and $4V_O$ systems (Table S8). Therefore, the energies related to these configurations in Figure 13a are marked as hatched bars.

The CO adsorption energies remained nearly unchanged for adsorption on the top layer terrace site, top layer edge site, middle layer site and interface (i) sites, regardless of the size of the O-vacancy cluster aside the Ru nanorod. In contrast, for adsorption on the interface (ii) site, there was a significant increase in CO adsorption energy upon the formation of the second O-vacancy in the $2V_O$ system.

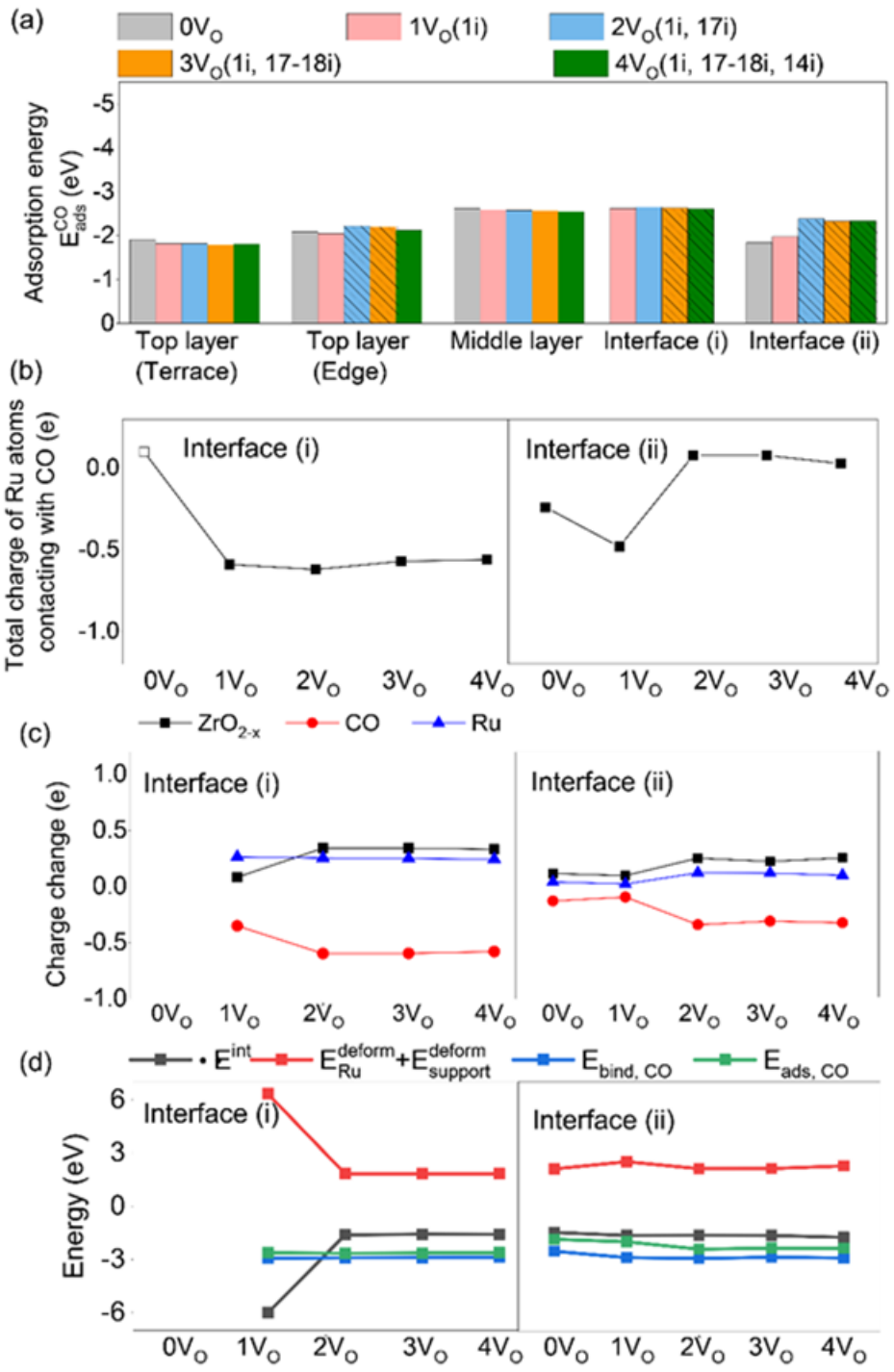

Figure 13. (a) CO adsorption energies on different sites on the fully oxidized, relaxed Ru/ZrO_2 (grey bar) and on the partly reduced, relaxed Ru/ZrO_{2-x} model systems with different O-vacancy clusters aside the Ru nanorod ($1V_O$: pink bar, $2V_O$: blue bar, $3V_O$: orange bar, and $4V_O$: green bar). (b) Total charge on the Ru atoms binding to CO on the interface (i) and interface (ii) sites before CO adsorption. (c) Change in charge state of the support (black squares and line), the Ru nanorod (blue triangles and line) and the CO molecule (red circles and line) upon CO adsorption on

interface (i) and interface (ii) site. d) Contributions from CO_{ad} induced deformation energies, change in interface energy and CO binding energy (see figure) to the total CO adsorption energy.

Analysis of the charge on the Ru adsorption site atoms before CO adsorption (Figure 13b and Table S34) and the changes therein for the Ru nanorod, support, and CO molecule (red dot and line) upon CO adsorption (Figure 13c) (see also Tables S35 – S37) revealed little variation of the charge on the top layer and middle layer sites (Table S34). The charge transfer to the CO molecule upon CO adsorption (Table S35) closely follows the trend in the charge on the Ru adsorption site before CO adsorption for the middle-layer sites, with a small charge transfer of below 0.1 e for CO adsorption at the middle layer site (Tables S34 and S35).

Little variation in the charge on the Ru adsorption site was found also for adsorption on the interface (i) site for the $1V_O$ – $4V_O$ systems (Table S38). As there is no stable adsorption on the interface (i) site for the fully oxidized system, the charge on this site is indicated by an open symbol. The generally higher charge on the interface (i) adsorption site compared to the middle layer site, mainly from the Ru-1a atom, does not seem to correlate with the about equal adsorption energies on both sites. This will be discussed further below in this section. Furthermore, we find an about constant charge transfer from Ru to the CO of about 0.25 e. In contrast, the charge transfer from the support to adsorbed CO increases significantly when going from the $1V_O$ to the $2V_O$ system, leading to a total charge transfer to the CO of about 0.59 e, which remains constant also at larger cluster sizes. Interestingly, the additional transfer from the support to CO when stepping from the $1V_O$ to the $2V_O$ system results only in a negligible increase in the CO adsorption energy, while for larger cluster sizes, the trends in charge transfer and CO adsorption energy are identical, despite the (small) change in CO adsorption site encountered for the $2V_O$ to 4 V_O systems (Table S8). The change in charge transfer from the $1V_O$ to the $2V_O$ system is accompanied also by a change in deformation and interface energies,

while the CO binding energy and the CO adsorption energy remain essentially constant (Figure 13d). Hence, there are significant structural and electronic changes upon formation of the second O-vacancy ($2V_O$ system), which, however, largely cancel out in their effect in on the CO adsorption energy.

For adsorption on the interface (ii) site, in contrast, we find an increase in (negative) charge upon formation of the first O-vacancy and a pronounced decrease when changing to the $2V_O$ system. This latter decrease goes along with a change in adsorption site, it mainly results from the much lower charge on the Ru-4a compared to the Ru-2a atom. While the initial increase follows the trend in adsorption energy, this is not the case for the subsequent decrease in charge. Most likely, the increase in adsorption energy is induced by the distinct reduction of the 1Zr surface ion upon formation of the O-vacancy at the 17i site (Table S38), which can contribute to the CO_{ad} bonding via direct Zr – CO interactions. This is reflected also by the abrupt increase in charge transfer to the CO molecule when going to the $2V_O$ system (Figure 13c), which stems mainly, but not exclusively from the oxide support (Figure 13c, Tables 38 and 40). For larger O-vacancy clusters, this does not change any more. Despite the rather small increase in total charge transfer from the support to the CO, the resulting energy gain seems to be enough to compensate for the loss of Ru-CO interaction. Finally, the data in Figure 13d illustrate that the CO adsorption energy largely follows the trend of the CO binding energy, indicating that changes in the CO_{ad} induced deformation energies and in interaction energies do not play a significant role. Also in this case, the difference between CO binding energy and CO adsorption energy is significantly larger than for adsorption on the interface (i) site, indicating that larger (positive) contributions from CO_{ad} induced deformation energies and changes in interface energies are mainly responsible for the lower adsorption energies on the interface (ii) sites.

Overall, these data support the trends derived in the previous cases. They clearly demonstrate that for a given adsorption site, the trend in the Ru-CO interaction depends on the charge on the

Ru adsorption site before CO adsorption and in particular on the Ru → CO charge transfer. Since there is no significant charge transfer to the top layer or middle layer sites, such variations are only possible on interface sites. The high adsorption energy on the Ru-5a middle layer site as compared to the top layer sites is again attributed to coordination effects, which play a role also for adsorption on the interface sites. The generally lower adsorption energy on the interface (ii) site is largely determined by a higher contribution from CO_{ad} induced deformation energies and changes in interface energies, as compared to adsorption on the other sites. Finally, mainly for adsorption on interface sites, interactions between a Zr surface ion and the adsorbed CO molecule can play an important role, if this ion is activated by a neighboring O-vacancy, either a single O-vacancy or a vacancy in an O-vacancy cluster.

3.2.3. Effect of O-vacancies in deeper layers underneath the Ru nanorod on the CO adsorption energy

Finally, we calculated the influence of O-vacancies in deeper layers underneath the Ru nanorod on the CO adsorption strength, using the same positions of the O-vacancies and adsorption sites as before (see section 3.1.3). The resulting CO adsorption energies are summarized in Figure 14a. When an O-vacancy is present at the (iv) site (indicated by the orange bar), the CO adsorbed at the edge site of the top layer (bridge site between 7a and 8a) will relax to the hollow site formed by 5a, 7a, and 8a Ru atoms, and CO adsorbed on the middle layer site (Ru-5a) will relax to a bridge site between 1a and 5a (Table S6). For adsorption on the interface (ii) site, the presence of an O-vacancy on the (ii) site causes the adsorbed CO to relax from the initial bridge site (Ru-2a, Ru-6a) to a bridge site formed by the Ru-2a and Ru-3a atoms. Furthermore, in this case CO adsorption also causes a spontaneous migration of the O-vacancy from the (ii) site to the (1i) site, where it is stabilized by interaction with the Ru nanorod. Therefore, the related energies are indicated as hatched bars in Figure 14a.

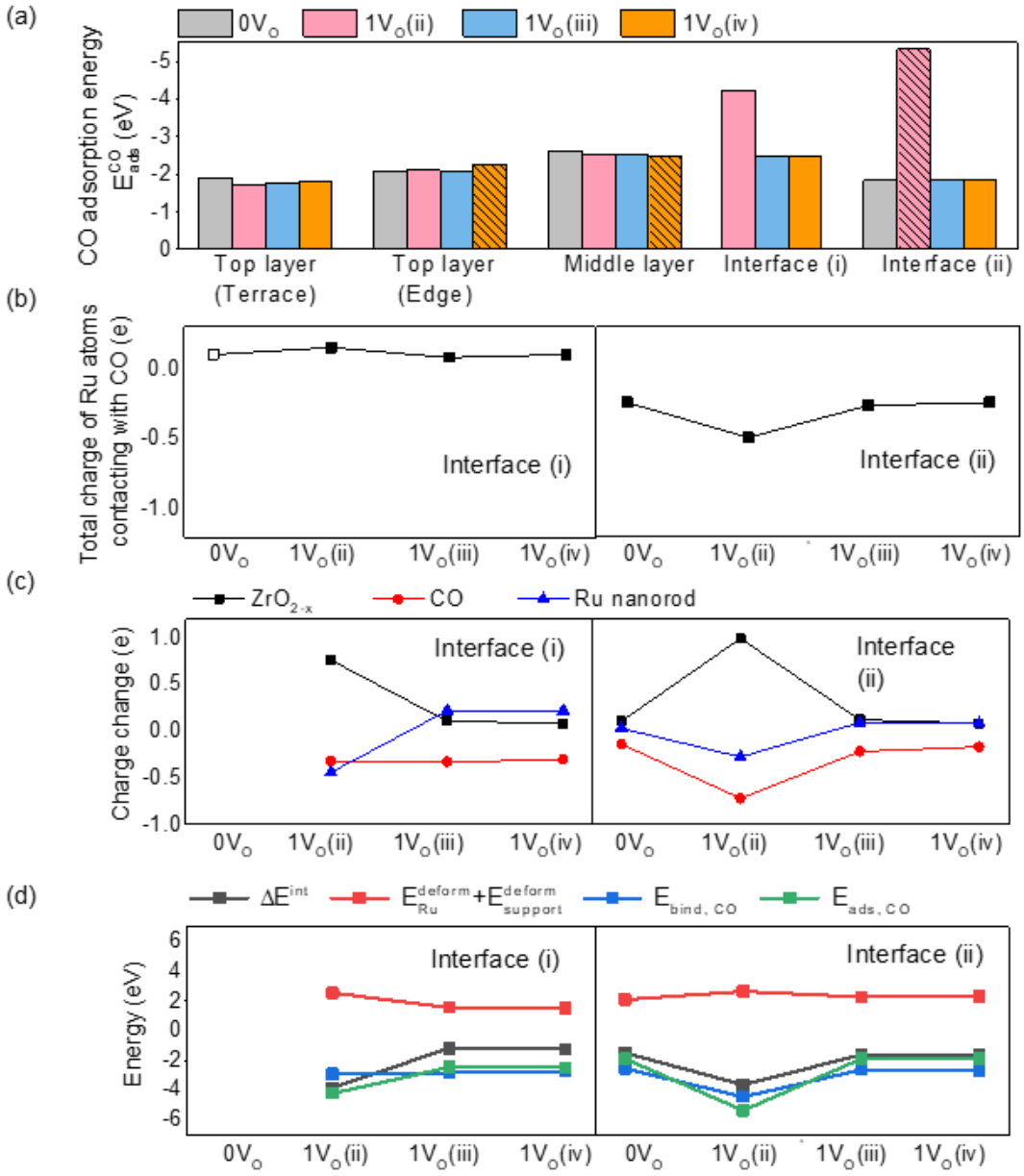

Figure 14. (a) CO adsorption energies on different sites on the fully oxidized, relaxed Ru/ZrO_2 (grey bar) and on the partly reduced, relaxed Ru/ZrO_{2-x} model systems with a single O-vacancy at the ii site (pink bar), iii site (blue bar), and iv site (orange bar). (b) Total charge on the Ru atoms binding to CO on the interface (i) and interface (ii) sites before CO adsorption. (c) Change in charge state of the support (black squares and line), the Ru nanorod (blue triangles and line) and the CO molecule (red circles and line) upon CO adsorption on the interface sites. d) Contributions from CO_{ad} induced deformation energies, change in interface energy and CO binding energy (see figure) to the total CO adsorption energy.

Similar to the effect of O-vacancies aside the Ru nanorod, O-vacancies in deeper layers have almost no influence on the CO adsorption strength, independent of the adsorption site. The only exception are O-vacancies in the second layer, at the (ii) site, which result in a significant increase of the CO adsorption strength on the two interface sites. Following our above explanation of the enhanced CO bond strength for adsorption on the interface site (ii) in the presence of a surface O-vacancy at the 16i site aside the Ru nanorod, the adsorption energy contains also contributions from a direct interaction between the adsorbed CO molecule and a partly reduced surface 1Zr ion neighboring to the O-vacancy on the (i) site. Note that the enhanced CO adsorption strength is observed only for CO adsorption on the two interface sites, not for adsorption on the middle layer site (Table S22). This is tentatively explained by the larger O(CO) − 2Zr distance (3.96 Å) on the middle layer site, while for CO adsorption at the interface (i) and (ii) sites, the distances to the closest Zr ion are only 2.34 Å (O(CO) − 2Zr) or 2.14 Å (O(CO) − 1Zr), respectively (Table S12). Furthermore, for adsorption on the interface sites, the CO adsorption energy also includes the gain in energy obtained upon the spontaneous migration of O-vacancy from the (ii) site to the (2i) site, where it is stabilized by interaction with the Ru nanorod.

This interpretation is supported by the results of the charge analysis on the Ru adsorption site and the charge transfer to the CO. Using the Ru adsorption sites listed in Table S6 for O-vacancies in deeper layers, we find little variation in the electron charge on the respective Ru adsorption sites, both for the interface (i) and interface (ii) adsorption site, except for a decrease on the interface (i) site and a significantly stronger increase for interface (ii) adsorption in the presence of an O-vacancy on the (ii) site (Figure 14b, Table S41). Hence, the much higher CO adsorption energy on the interface (i) site of the $1V_O$(ii) system is not reflected by a higher charge on this Ru adsorption site, while for adsorption on the interface (ii) site these trends would be comparable. For adsorption on the interface (ii) site, the increase in charge on the

adsorption site results. For both sites, the changes in charge are reversed again for deeper lying O-vacancies.

Inspection of the charge on the 1Zr and 2Zr surface ions, however, which as discussed before can interact with the CO adsorbed on the interface sites, reveals distinct charge changes (Table S41). Both ions, in particular the 1Zr ion, are partly reduced for an O-vacancy at the (ii) site. This can be rationalized by their shorter distances to the O-vacancy of 2.27 Å (1Zr) and 2.49 Å (2Zr), respectively, while for the O-vacancies on the (iii) and (iv) sites these distances are much larger (Table S18). Apparently, the very high CO adsorption energies at the interface (i) and (ii) sites in the presence of an O-vacancy on the (ii) site are mainly caused and dominated by an additional direct interaction between the O atom of the adsorbed CO and the 1Zr and 2Zr surface ions, respectively, overriding the effects caused by the charge on the Ru adsorption site.

The changes in charge of the CO, of the support, and of the Ru nanorod upon CO adsorption at interface (i) and (ii) sites for the different O-vacancy locations as well as for the fully oxidized system ($0V_O$) are illustrated in Figure 14c. Generally, there is a higher charge transfer to the CO for adsorption on the interface (i) site than for the interface (ii) site, which fits to the generally higher CO adsorption energy in the former case, but differences between different O-vacancies are small. Only for adsorption on the interface (ii) site in the presence of an O-vacancy on the (ii) site there is a much more pronounced charge transfer to the CO (Figure 14c). This is likely related to the change in adsorption site for this system, from Ru-2a / Ru-6a to Ru-2a / Ru-3a (Table S6), and in fact could provide the driving force for it.

Inspection of the charge change on the Ru nanorod and on the support reveals additional details. For both adsorption sites there are pronounced changes only in the presence of an O-vacancy on the (ii) site. For CO adsorption on the interface (i) site, this is mainly a CO induced charge transfer from support to the Ru nanorod, while the charge change on the CO is similar to that in the other systems. For CO adsorption on the interface (ii) site, in contrast, we find a

considerable charge transfer from the support both to the Ru nanorod and to the adsorbed CO, which both become more negative. Hence, the contributions from the charge transfer to the increase in CO adsorption energy on the two interface sites in the presence of an O-vacancy on the (ii) site are different, although it involves in both cases a charge transfer from the support upon CO adsorption, once to the Ru nanorod and once to both Ru nanorod and CO.

Here it is interesting to note that the direct interaction of the adsorbed CO with the closest Zr surface ion does not only cause a change in charge state of this Zr ion, but affects also the other Zr ions surrounding the O-vacancy. For example, CO adsorption on the interface (i) site leads to a re-oxidation not only of the 2Zr ion from +2.34 e to +2.59 e, but also of the 1Zr ion (from +2.17 e to +2.46 e) and of the other two Zr ions surrounding this O-vacancy (Tables S41 and S42) Hence, while the interaction between CO and Zr surface ion is considered to be highly local, polarization effects can also modify the charge on more distant ions.

The differences in CO adsorption energies on the interface (ii) site on the one hand and on the interface (i) site and the middle layer site on the other hand are again mainly due to larger (positive) contributions from the CO_{ad} induced deformation energies and changes in the interface energies, which are reflected by the larger difference between CO binding energy and CO adsorption energy (Figure 14d). These change little upon variation of the O-vacancy position, except in the presence of the O-vacancy on the (ii) site. In this case, both the CO binding energy as well as the sum of deformation and interface energies contribute to the higher CO adsorption energies (Figure 14d).

Finally, we would like to note that while in the previous section we could not distinguish whether CO adsorption is stabilized by direct interaction with the O-vacancy center or by interaction with the partly reduced neighboring Zr surface ion, in the present case a direct interaction of the adsorbed CO molecule with the O-vacancy in the second layer is unlikely.

Therefore, this stabilization must be due to the stronger additional interaction of the adsorbed CO with a closely neighbored partly reduced Zr surface ion.

Effect of O-vacancy clusters: The influence of O-vacancies in O-vacancy clusters in deeper layers underneath the Ru nanorod on the CO adsorption energy is illustrated in Figure 15a (see also Table S23). Starting with an O-vacancy on the (1i) site ($1V_O$), the vacancy cluster grows by formation of additional O-vacancies at the neighboring ii, iii, and iv sites in deeper layers, with the resulting systems being denoted as $2V_O$, $3V_O$, and $4V_O$. Also in this series we have to consider a few changes in adsorption site / behavior. During optimization, CO adsorbed on the edge site of the top layer relaxes to a hollow site formed by the 7a, 8a, and 5a Ru atoms in the $2V_O$ and $4V_O$ systems (Table S8). CO adsorbing on the interface (i) site in the $2V_O$ system dissociates into C and O. Therefore, the related CO adsorption energy is not included in Figure 15a. For the $3V_O$ and $4V_O$ systems, CO adsorbing at the interface (i) site (1a, 5a) relaxes to a threefold hollow site formed by the Ru-2a, Ru-4a and Ru-5 atoms (Table S8) (hatched bars in Figure 15a). Furthermore, CO adsorbed at the interface (ii) site relaxes to a bridge site composed of 4a and 6a for the $2V_O$ – $4V_O$ systems (Table S8) (hatched bar in Figure 15a).

Similar to the results for a single O-vacancy at different positions underneath the Ru nanorod (Figure 14a), the effect on the adsorption energy of CO on the top layer and the middle layer site is negligible. Adsorption at the middle layer site is again slightly more stable than on the top layer site, which we explained before by the lower coordination of the Ru-5a atom in the middle layer. An essentially constant adsorption energy is obtained also for adsorption on the interface (i) site, with the exception that there is no stable adsorption on this site for the $0V_O$ and $2V_O$ systems, where CO_{ad} either moves to the middle layer site ($0V_O$ system) or dissociates ($2V_O$ system). Formation of an O-vacancy on the 1i site stabilizes CO adsorption on the interface (i) site, with an adsorption energy similar to that on the middle-layer site. Synergistic effects are observed upon formation of a second O-vacancy on the (ii) site. While a single O-

vacancy on this site results only in a change of the adsorption site (Figure 14a), the presence of an additional O-vacancy at the 1i site causes a dissociation of the CO. Formation of additional O-vacancies in the $3V_O$ and $4V_O$ systems causes little change in charge state of the adsorption site (Figure 15b) and does not lead to CO dissociation any more. Hence, similar as for the individual O-vacancies in deeper layers (Figure 14b), the additional O-vacancies do not affect the charge on this adsorption site in an O-vacancy cluster. A similar trend is observed also for the charge transfer between CO, Ru nanorod and support (Figure 15c), with a rather constant transfer of about - 0.35 e to CO adsorbed on the interface (i), both from the Ru and from the support. This seems to be dominated by the presence of the O-vacancy at the 1i site, with little effect from additional, deeper lying O-vacancies. Finally, Figure 15d indicates that the CO adsorption energy largely follows the CO binding energy. Hence, the pronounced changes in the deformation and interface energies observed for the $1V_O$ system essentially cancel out.

Finally, considering adsorption on the interface (ii) site, the formation of the O-vacancy at the 1i site results in a significant increase of the negative charge on the Ru adsorption site (Figure 15b), comparable to that of an individual O-vacancy at the (ii) site (Figure 14b). Addition of an O-vacancy at the (ii) site, however, does not further increase the negative charge on this adsorption site, but changes it to a slightly positive value. This is at least partly related to the different adsorption sites in both cases, a (Ru-2a, Ru-6a) bridge site for the individual (ii) O-vacancy and a (Ru-4a, Ru-6a) bridge site for the (ii) O-vacancy in the $2V_O$ vacancy cluster. Further addition of deeper lying O-vacancies does not change this situation any more.

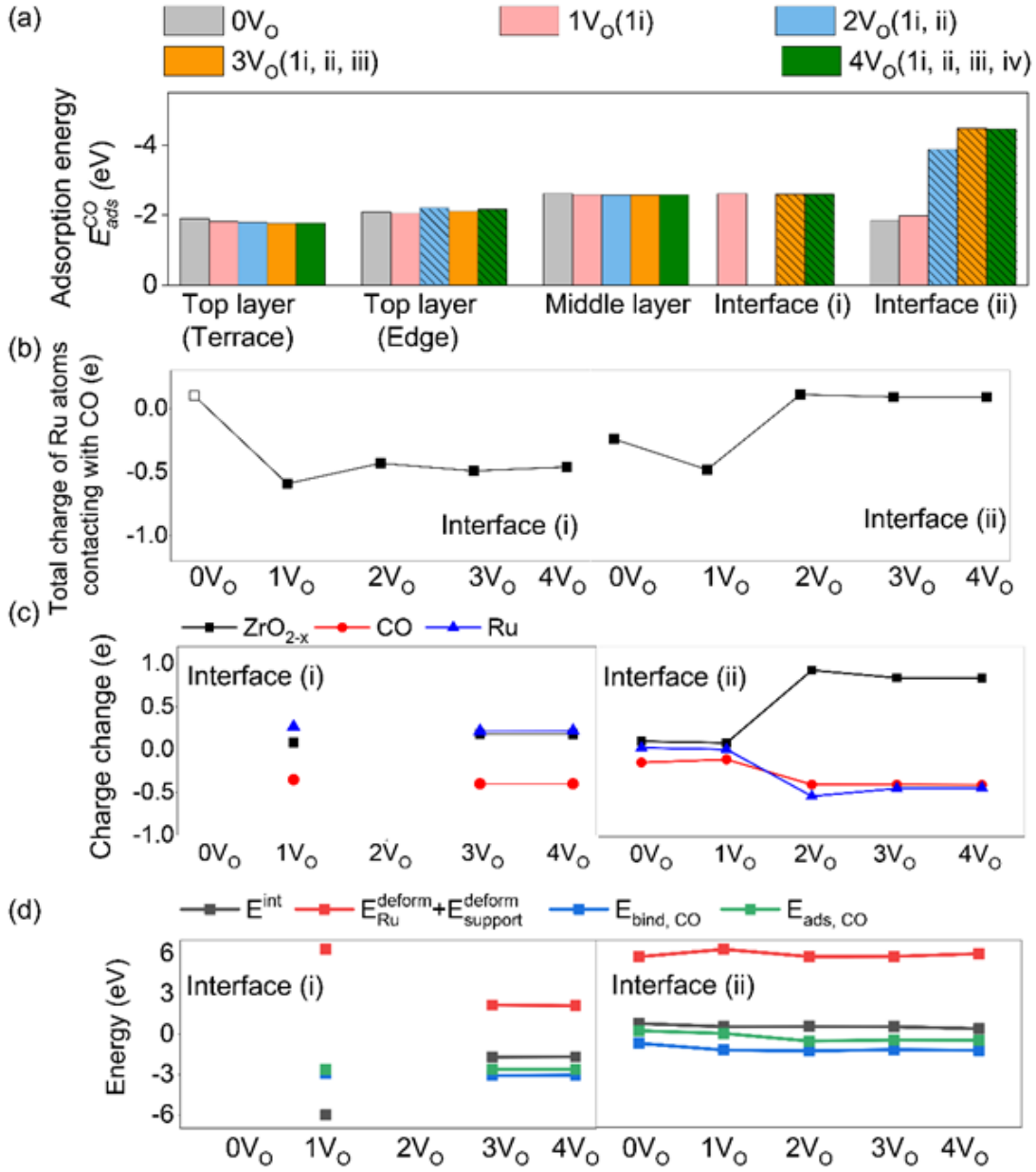

Figure 15. (a) CO adsorption energies on different sites on the fully oxidized, relaxed Ru/ZrO_2 (grey bar) and on the partly reduced, relaxed Ru/ZrO_{2-x} model systems with different O-vacancy clusters aside the Ru nanorod ($1V_O$: pink bar, $2V_O$: blue bar, $3V_O$: orange bar, and $4V_O$: green bar). (b) Total charge of Ru atoms binding to CO on the interface (i) and interface (ii) sites. (c) Charge change of the support (black dots and line), the Ru nanorod (blue dots and line) and the CO molecule (red dots and line) upon CO adsorption on the interface sites. d) Contributions from CO_{ad} induced deformation energies, change in interface energy and CO binding energy (see figure) to the total CO adsorption energy.

The charge transfer upon CO adsorption on the interface (ii) site is initially small, both for the fully oxidized system and $1V_O$ system with the O-vacancy at the 1i site. Formation of the (ii) vacancy in the $2V_O$ system results in a distinct re-oxidation of the support, in particular of the 1Zr and 2Zr surface ions (Tables S44 and S46), but also of the other Zr ions around this vacancy, if these were partly reduced upon formation of the O-vacancy. Additional formation of the deeper lying (iii) and (iv) O-vacancies does not change this situation any more, which is in full agreement with the little changes in the CO adsorption energy and in the charge on the adsorption site for these systems. Finally, the tendency towards higher CO adsorption energies for the $2V_O$ and larger clusters (Figure 15a) partly results from an increase in CO binding energy, but in this case contributions from the interface and deformation energies also play a role (Figure 15d).

Hence, also in the case of deeper lying O-vacancies their effect on the CO adsorption energy is rather small, with the only exception in cases where the CO molecule can interact with a suitably positioned Zr surface ion, which due to a neighboring O-vacancy is partly reduced. This allows stronger CO bonding even in the absence of significant electron charge on the Ru adsorption site. Also in this case, the differences in adsorption energy on the different adsorption sites can again be attributed to larger (positive) contributions from CO_{ad} induced deformation energies and changes in the interface energies, which are reflected by larger differences between CO binding energy and CO adsorption energy, and to coordination effects. The latter are responsible for the generally higher adsorption energies on the middle layer Ru-5a site and partly for the higher energy on the interface sites, the former result in lower CO adsorption energies for adsorption on interface (ii) sites than on interface (i) sites, counteracting coordination effects.

3.2.4 CO_{ad} induced lowering of the O-vacancy formation energy

The data presented in the previous sections indicated that adsorbed CO will lower the energy for O-vacancy formation, which is defined as the difference of the O-vacancy formation energy in a Ru/ZrO_2 model system with an adsorbed CO ($E_{vac,Ru/ZrO2+CO}$) and in the CO_{ad}-free Ru/ZrO_2 model system ($E_{vac,Ru/ZrO2}$). In that case, the CO_{ad}-induced lowering of the O-vacancy formation $\Delta E_{vac,CO}$ can be determined as

$$\begin{aligned}\Delta E_{vac,CO} &= E_{vac,Ru/ZrO2+CO} - E_{vac,Ru/ZrO2} \\ &= -E_{ad,Ru/ZrO2} + E_{vac,Ru/ZrO2} + E_{ad,,Ru/ZrO2-x} - E_{vac,Ru/ZrO2} \\ &= E_{ad,Ru/ZrO2-x} - E_{ad,Ru/ZrO2} \end{aligned} \quad (5)$$

where $E_{ad,Ru/ZrO2}$ and $E_{ad,Ru/ZrO2-x}$ describe the CO adsorption energies on the same Ru/ZrO_2 model system and on the partly reduced Ru/ZrO_{2-x} system on the same Ru site. Considering that CO adsorption is generally stronger on the partly reduced system, adsorbed CO will generally result in a lowering of the O-vacancy formation energy.

We would like to note that in this relation we only considered adsorption of a single CO on the same site in both cases. But we would expect a similar trend also for adsorption of several CO molecules. On the other hand, considering practical applications, one needs to keep in mind that O-vacancy formation requires considerable energy and thus will proceed only at sufficiently high temperatures. Under these conditions, adsorbed CO is likely to desorb, resulting in very low steady-state coverages. Hence, a CO_{ad}-induced lowering of the O-vacancy formation energy can only be observed at sufficiently high CO partial pressures, which allow for a measurable steady-state CO_{ad} coverage.

3.2.5 Correlation between charge on the Ru atoms binding with CO and CO adsorption energy

The previous sections indicated a clear correlation between the charge on the Ru adsorption site, i.e., on the Ru atoms contributing to the Ru-CO bond, and the CO adsorption energy for CO adsorption on the interface sites. For adsorption on the top layer and middle layer sites, where due to the metallic screening the charge on the Ru atoms changes little upon O-vacancy formation, O-vacancy induced changes in the CO adsorption energy are generally very small. For adsorption on the interface sites, where CO binds to Ru atoms in the bottom layer (interface layer), whose charge state varies significantly with the position of the O-vacancies and the size of O-vacancy clusters, the variations of the CO adsorption energy are more significant. To test for a general correlation between charge state of the Ru adsorption site and the CO adsorption energy, we plotted the CO adsorption energy on the interface sites as a function of the charge state of the Ru adsorption site. Figure 16 illustrates the correlation between these properties for various different O-vacancy positions and O-vacancy cluster sizes for CO adsorption on the interface (i) site (Figure 16a) and on the interface (ii) site (Figure 16b). In these plots we did not consider those cases where as discussed in sections 3.2.1 – 3.2.3 the adsorption energy includes either changes in the O-vacancy position or direct interactions between CO and Zr surface ions.

Figure 16a reveals a linear relationship between the CO adsorption energy and the total charge on the Ru atoms binding to CO on the interface (i) site. In this plot, we did not include the data points for O-vacancies on the 16i site aside the Ru nanorod ($1V_O$(16i)) and on the (ii) site in the second layer below the Ru nanorod ($1V_O$(ii)), where a direct interaction between the O atom of the CO molecule and a partially reduced Zr surface ion located near the O-vacancy leads to an additional stabilization of the adsorbed CO. For adsorption on this site, the variation of the CO adsorption energy with the charge state of the Ru adsorption site is rather small, reflected by a

small slope of the fit to the data (red line). The only significant deviation from the fit line occurs for CO adsorption on the interface (i) site with a $5V_O$ O-vacancy cluster in the topmost layer underneath the Ru nanorod, where the CO adsorption energy is less than expected from the linear correlation.

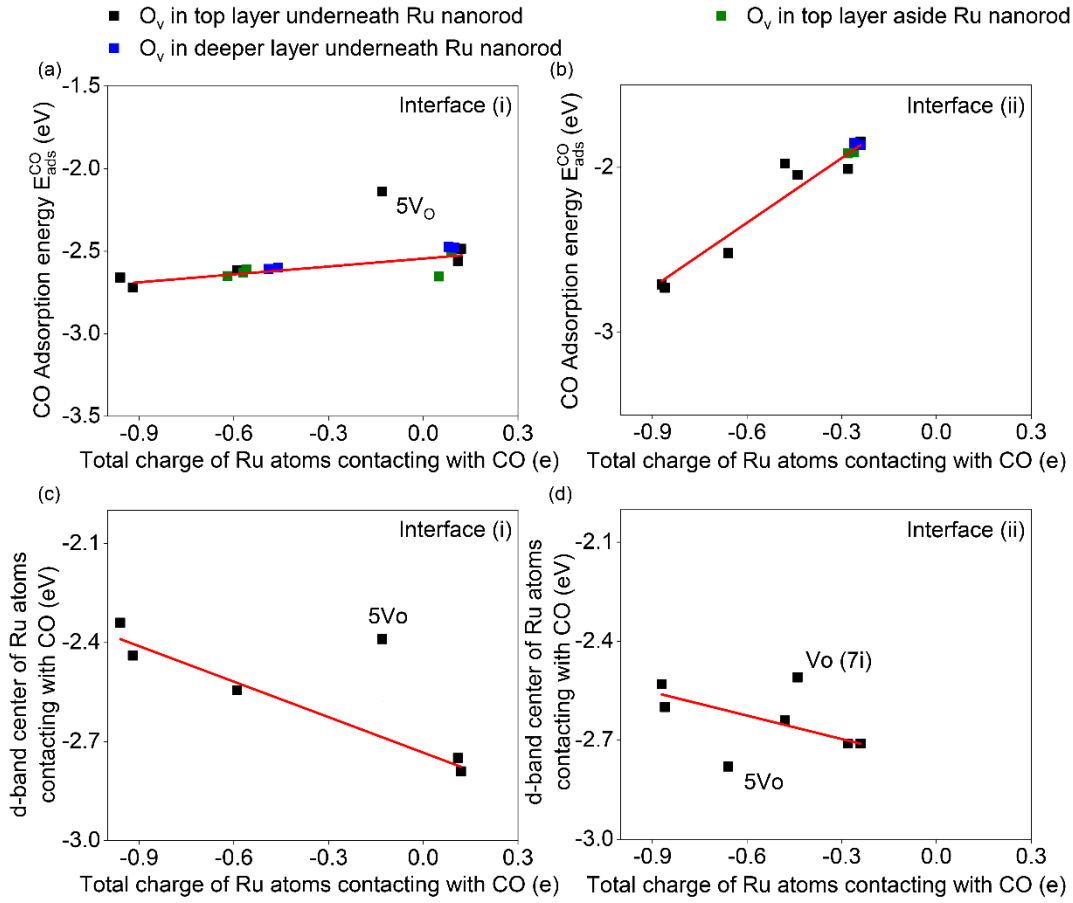

Figure 16. Plots of the CO adsorption energies (a, b) and the center of the d-band density of states (c, d) on interface (i) (a, c) and (ii) (b, d) sites as a function of the total charge on the Ru atoms binding with CO for individual O-vacancies or O-vacancy clusters in the top and deeper layers. The red lines represent fits to the adsorption energies, center of the d-band and charge data in Figures 10-15. Not included in these plots are those cases where the adsorption energy includes either changes in the O-vacancy position or direct interactions between CO and Zr surface ions (see sections 3.1.1. – 3.1.3).

According to the analysis of the contributions from the CO_{ad} induced deformation of the Ru nanorod (E_{Ru}^{deform}) and of the support ($E_{ZrO_{2-x}}^{deform}$), from the change in interface energy in the presence of adsorbed CO ($\Delta E_{Ru-support}^{int}$) and finally the actual CO binding energy on the relaxed adsorption site ($E_{bind,CO}$), the lower CO adsorption energy for CO adsorption on a Ru/ZrO_{2-x} system with a $5V_O$ vacancy cluster underneath the Ru nanorod is partly due to a significant (positive) contribution from the sum of the CO_{ad} induced deformation energies and change in interaction energies, which is around 0.4 eV, which leads to a lowering of the CO adsorption energy (Table S27). In addition, also the CO binding energy is lower than in other cases.

For CO adsorption on the interface (ii) site, we also find a linear correlation between charge on the adsorption site and CO adsorption energy. Also for this fit, we did not include the cases with significant contributions from direct interactions between CO and partly reduced Zr surface ions or CO_{ad} induced migration of the O-vacancy (see discussion in sections 3.2.1 – 3.2.3). Interestingly, for adsorption on this site the slope of the fit line is much steeper than obtained for adsorption on the interface (i) site. Apparently, CO adsorption on this site is much more sensitive to changes in the charge on the Ru adsorption site than adsorption on the interface (i) site. We will get back to this in a moment.

Similar plots of the center of the d-band density of states vs. the charge on the Ru adsorption sites (Figure 16c, d) lead to almost identical results, with a linear correlation between these parameters. Hence, a more negatively polarized Ru adsorption site results in an upshift of the d-band center. Interestingly, in this case the difference in slopes between interface (i) and interface (ii) sites is much less than for in the plots of the adsorption energy adsorption (Figure 16a, b). In combination, this reflects the experience that the energy of the center of the d-band LDOS affects the CO adsorption energy to different extents, depending on the nature of the material and the exact adsorption site.[45;46] The few systems which deviate from this linear

correlation are partly the same as in Figures 16a, b, namely the $5V_O$ system for both interface sites, and the $1V_O$(7i) system for adsorption on the interface (ii) site. All of these cases involve a change in adsorption site, which affects the calculation of the charge and of the d-band center on the adsorption site by addition/removal of specific Ru atoms. Hence, most simply, these deviations are due to limitations in the simple averaging procedure of these values for adsorption sites with several surface atoms contributing.

In total, the data presented in this section 3.2 result in the following picture: O-vacancies in the support generally stabilize CO adsorption on the Ru nanorod in cases where O-vacancy and Ru adsorption site are in direct contact, with distances of 2 Å and less, which allows significant charge transfer from the O-vacancy to the neighboring Ru interface atoms. Hence, such effects are essentially limited to CO adsorption at the interface sites and O-vacancies in the support in direct contact to the Ru nanorod, while for adsorption at higher layers, at top-layer or middle-layer sites, charge transfer is inhibited due to the very effective metallic screening by the interface layer. The O-vacancy induced stabilization of CO adsorbed on a given site is essentially linearly related to the charge on the Ru adsorption site, which allows a more pronounced charge transfer to the adsorbed CO molecule and thus results in a strengthening of the Ru – CO bond, and also to the shift in the center of the d-band LDOS on the adsorption site.

CO adsorption on the top layer sites largely resembles more that on metal surfaces, where the coordination of the adsorption site plays a dominant role. Due to metallic screening, charge transfer from the support to these adsorption sites is negligible, and the energy of the d-band center is rather low below the Fermi level (Table S48 and S53). Contributions from CO_{ad} induced deformation and changes in the interface energies are small or negligible as well. Furthermore, due to their distance, direct interactions between CO and Zr surface ions can be neglected as well.

For CO adsorption on the interface sites, charge transfer from the support can be significant, in particular for O-vacancies that are neighbored to the Ru adsorption site, and can lead to a higher CO binding energy and an up-shift in d-band center. Furthermore, contributions from the CO_{ad} induced deformation energies and changes in interface energies can be significant as well. In the present case, they lead to a general lowering of the CO adsorption energy on the interface (ii) sites compared to the interface (i) sites, to the level of CO adsorption energies on the top layer sites. Both, charge and coordination have less effect on the CO adsorption energy on the interface (i) sites than on the interface (ii) sites. Finally, depending on the position of the O-vacancy, CO_{ad} can directly interact with a partly reduced Zr surface ion neighboring to an O vacancy, which can lead to large increases in the CO adsorption energy.

CO adsorption on middle layer sites, in this case specifically on the Ru-5a adsorption site, is in between these previous two cases. Charge transfer to this site is small and hardly affected by O-vacancies. Also, contributions from CO_{ad} induced deformation energies and changes in interface energies, which could lower the adsorption energy, are mostly small. Coordination effects and the resulting up-shift in d-band center are the main driver for the higher adsorption energy on this site compared to adsorption on top layer sites. On the other hand, in some cases adsorbed CO can directly interact with partly reduced Zr surface ions (see Figure 12b), which leads to an abrupt increase of the CO adsorption energy and can also induce a change in adsorption site during relaxation. Thus, the similar size of the increase in CO adsorption energy for adsorption on the middle layer site and on the interface (i) site is fortuitous and does not result from identical effects. The same is true also for adsorption on the top layer sites and on the interface (ii) site.

Based on these data, we propose that the adsorption energies on such kind of supported metal systems are generally affected by a number of different contributions:

- Adsorption on sites away from the interface is dominated by coordination effects, which can be captured by the energy of the d-band center of the adsorption site, in the framework of the d-band model.
- O-vacancy induced charge transfer to Ru surface atoms and accordingly charge induced variations in the CO adsorption energy are negligible for Ru adsorption sites and/or O-vacancies away from the interface, while for interface sites they can be substantial, depending on the position of the O-vacancy.
- CO_{ad} induced deformation energies and changes in the interface energies are particular important for adsorption at interface sites, where they can dominate changes in the adsorption energy, while for adsorption on higher layer sites their combined contribution is small.
- Direct interaction between CO and a partly reduced surface cation neighbored to an O-vacancy can lead to drastically increased adsorption energies and in the present case even to CO dissociation.

While the numbers may differ for other systems, this overall picture is proposed to be of general validity. This also means that predictions solely based on the d-band model, using the energy of the d-band center of the adsorption site as descriptor, are likely to fail, as they do not include these other effects that are highly important in particular for adsorption on interface sites.

Finally, we demonstrated that adsorbed CO leads to a stabilization of oxygen vacancies and hence to a lowering of the O-vacancy formation energy.

3.3 C-O vibrational properties

For further information on the CO adsorption behavior and on the effect of O-vacancy formation thereon we also evaluated the C-O vibrational properties. Here we focused on those cases where the adsorption energies indicate a significant effect of the O-vacancies. Therefore,

the cases of O-vacancies aside the Ru nanorod or in deeper layers underneath the nanorod were not considered. In the left panel of Figure 17 we illustrate trends in the C-O frequencies for CO adsorption on the different Ru sites discussed before, including top layer terrace sites (black), top layer edge sites (red), middle layer sites (blue), interface (i) sites (green) and interface (ii) sites (orange). Frequencies were calculated for CO adsorbed on the fully oxidized Ru/ZrO_2 model system and on the partly reduced Ru/ZrO_{2-x} systems with a single O-vacancy located at representative sites in the first row (1i site), second row (4i site) or third row (7i site) underneath the Ru nanorod (see Figure 2), where CO adsorption was most stable. Adsorption on the fully oxidized Ru/ZrO_2 is denoted in these panels as the 0^{th} row and $0V_O$-vacancy cluster. As evident from Figure 17, the CO molecules adsorbed on the top layer terrace sites and, except for the fully oxidized system, at the middle layer exhibit the highest vibrational frequencies, which fits well to the generally higher frequencies of CO adsorbed on on-top sites. For adsorption on the top layer edge site the frequencies are generally lower, as expected for adsorption on bridge sites (see Tables S6 and S7). Changes in the frequencies with O-vacancy position are either fully absent (top layer terrace sites) or small (top layer edge sites). This fully agrees with expectations based on the constant adsorption energies and charges on the top layer sites due to metallic screening. For adsorption on the middle layer site we find a distinct up-shift by about 160 cm^{-1} when introducing an O-vacancy, independent of the position of the vacancy. This change in vibrational frequency is much more pronounced than the small increase in CO adsorption energy on this site (see Figure 10). It may be related to a change in the orientation of the adsorbed CO adsorbed. In the $0V_O$ configuration, CO points downward towards one Zr surface ion in the support, while in the presence of an O-vacancy the C-O bond is parallel to the support surface. While a simple explanation of the physical origin for this change in orientation is still missing, it nevertheless demonstrates the complexity of these adsorption systems.

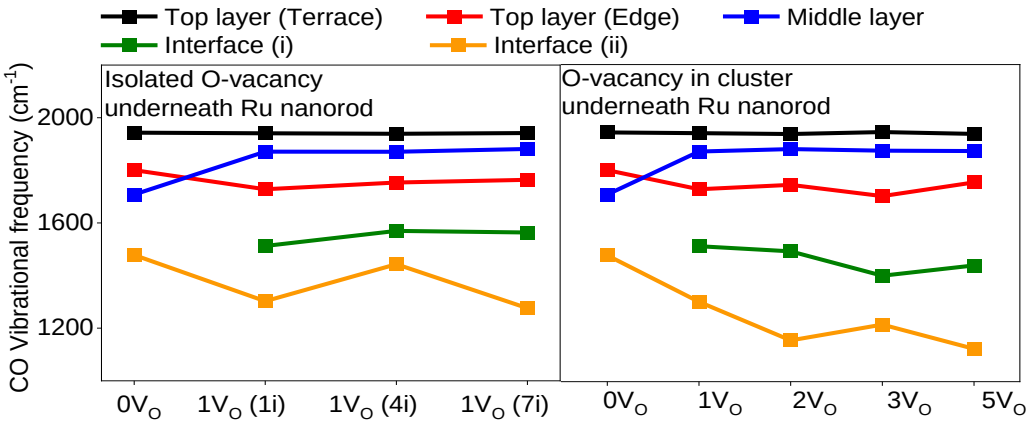

Figure 17. C-O vibrational frequencies of CO adsorbed at the Ru sites indicated in the figure for different positions (1st row: 1i, 2nd row: 4i, 3rd row: 7i O-atom) of individual O-vacancies underneath the Ru nanorod (left panel) and for O-vacancies in a growing O-vacancy cluster (right panel).

Adsorption on the interface sites results in the lowest frequencies, as expected for CO adsorption on bridge or threefold hollow sites. For adsorption on the interface (i) site, the vibrational frequency is lower than expected for adsorption on bridge sites (see Table S6), which may be related to the additional interaction with the 2Zr surface ion. Here we find a small increase of the C-O frequency when moving the O-vacancy away from the adsorption site, from the 1st to the 2nd and then to the 3rd row. (There is no stable CO adsorption on this site in the absence of an O-vacancy). The small upshift of about 57 cm^{-1} fits well to the subtle decrease in CO adsorption energy (see Figure 10b). Both trends are related to the decreasing electron charge transfer (see Figure 10a) to the adsorption site upon O-vacancy formation with increasing distance of the vacancy from the adsorption site.

The lowest vibrational frequencies and the most significant changes of the C-O vibrational frequency with increasing distance between adsorption site and O-vacancy position are observed for adsorption on the interface (ii) site. The very low frequencies must be due to the additional interaction of the adsorbed CO molecule with the 1Zr surface ion. The zig-zag behavior of the C-O frequency seems to follow the trend in the charge on the Ru adsorption

site, which varies from -0.24 e via -0.48 e and -0,28 e to finally -0.44 e (Figure 10c). This is different for the CO adsorption energy, which shows a very small steady increase (Figure 10b). The discrepancy between the trends for CO adsorption energy and C-O frequency is most likely due to the additional interaction of the CO with the 1Zr ion

Changing to modifications in the CO vibrational properties upon formation of O-vacancies in a growing O-vacancy cluster underneath the Ru nanorod we find no significant differences to the effect induced by individual O-vacancies for CO adsorption on the top layer and middle layer sites, consistent with the generally weak effects of the O-vacancies on CO adsorbed on these sites (Figure 17, right panel).Note that in this case neighbored O-vacancies had to be considered to simulate a growing O-vacancy cluster (O-vacancies at position 1i, 2i 3i, 4i, 5i). For adsorption on the middle layer site, the presence of an O-vacancy on the 1i site ($1V_O$ system), which is present also in the larger clusters, is sufficient to induce the up-shift of the vibrational frequency, and this does not change any more for larger O-vacancy islands.

For adsorption on the interface (i) site, the slight up-shift of the frequency with increasing distance between O-vacancy and CO adsorption site, from the 1i to the 4i site (see left panel, Figure 17), which was observed for individual O-vacancies, changes into a more pronounced down-shift for the growing O-vacancy cluster, from the $1V_O$ to the $2V_O$ and in particular the $3V_O$ system (see right panel, Figure 17). This goes along with a considerable increase of the electron charge on the Ru adsorption site (Figure 11b) and a slight decrease/increase of the charge transfer to the adsorbed CO for the $2V_O$/$3V_O$ system (Figure 11c). The latter trend agrees with decrease in C-O vibrational frequency upon increasing charge transfer to the CO. Similar agreement in trends is also obtained upon formation of the 4^{th} and 5^{th} vacancies ($5V_O$ system), where a slightly increasing charge C-O frequency correlates with a slightly decreasing charge transfer.

Finally, for CO adsorption on the interface (ii) site, which also for O-vacancy cluster shows the lowest C-O vibrational frequencies and the most pronounced changes with increasing size of the O-vacancy cluster, the trend of a decreasing C-O vibrational frequency (Figure 17, right panel) correlates well with the increasing charge and charge transfer to the adsorbed CO molecule up to the formation of the second O-vacancy ($2V_O$) (Figure 11c), Upon formation of the third O-vacancy this agreement ceases, as the subtle increase of the vibrational frequency goes along with an essentially constant charge transfer to the adsorbing CO molecule (Figure 11c). Most likely, this is due to a change in the CO – 1Zr interaction, although there is no obvious change in the charge state of that ion. Finally, for the $5V_O$ system, this discrepancy is even more pronounced, since a clear decrease in C-O vibrational frequency goes along with an essentially constant charge transfer to the adsorbing CO, different from expectations based on the Blyholder picture.

In general, these trends in the vibrational frequencies support the conclusions drawn from the CO adsorption energies that the presence of O-vacancies has significant impact on the CO adsorption properties in cases where CO is adsorbed on interface sites, which are directly affected by charge transfer from the support to the Ru nanorod, and that the effects increase for close distances between O-vacancy and adsorption site. They mostly agree with the trend expected from the Blyholder picture, where an increasing charge transfer to the adsorbing CO molecule results in a decreasing C-O vibrational frequency, due to an increasing population of the antibonding $2\pi^*$ orbital. Deviations from the expected trends are observed in configurations with significant interactions between CO and partly reduced Zr surface ions adjacent to O-vacancies.

Conclusions

As part of our comprehensive study of electronic metal−support interactions (EMSIs) and their effect on the adsorption properties of oxide supported metal catalysts, we have continued to investigate O-vacancy formation energetics on Ru/ZrO_2 model catalysts and their impact on CO adsorption by DFT calculations. Employing a model system consisting of a $ZrO_2(111)$ support and a three-layer $[11\bar{2}0]$ oriented Ru nanorod, we have systematically evaluated the impact of the position of the O-vacancy relative to the Ru nanorod on the vacancy formation energy and its effect on CO adsorption properties. The main findings of these calculations are as follows:

- Energetically, O-vacancy formation is significantly relieved mainly at interface sites, where the O atom is in direct contact with the metal nanorod. Significant stabilization is observed for O-vacancies close to a Ru interface atom, at distances about 2 Å, where it can reach up to 2.8 eV. For O-vacancy formation in deeper layers below the Ru nanorod or aside the nanorod the stabilization of the O-vacancy is very small or absent, i.e., its formation is comparable to vacancy formation in the absence of the metal nanorod.
- The Ru induced stabilization of the O-vacancies is closely correlated with the charge transfer from the support to the Ru nanorod upon O-vacancy formation.
- Considering also kinetic effects, O-vacancy formation occurs preferentially at the interface perimeter sites, at the edge of the Ru nanorod. Subsequent O-vacancy migration can lead, however, to O-vacancies at more central positions underneath the Ru nanorod, which are of comparable stability. Generation of surface vacancies away from the interface or in deeper layers and their accumulation are energetically unfavorable.
- These trends are valid also in the presence of neighboring O-vacancies, in a growing O-vacancy cluster. The O-vacancy formation energy on a given site is generally little affected by the presence or absence of neighboring O-vacancies in a growing O-vacancy cluster.

- CO adsorption is mainly affected by O-vacancies if these and the Ru adsorption site are in direct contact, i.e., for adsorption at interface layer Ru atoms/sites and the O-vacancies at the perimeter of the Ru nanorod. The CO adsorption energy is increased by an O-vacancy enhanced charge transfer to the Ru adsorption site and, correlated with that, an increased charge transfer from the metal to the adsorbing CO molecule. For adsorption at higher layers or in the presence of more distant O-vacancies, metallic screening hinders charge transfer to the adsorption site.
- In addition to this effect, which dominates the CO adsorption energies on the same adsorption site, but with O-vacancies at different positions, CO adsorption can also be affected by i) contributions from CO_{ad} induced deformation energies and changes in interface energies, by ii) differences in the coordination of the adsorption site, and in particular by iii) the interaction with Zr surface ions that are partly reduced due to charge transfer from a neighboring O-vacancy. Since this latter charge transfer is very local, such effects are limited to specific O-vacancy sites close to the Ru perimeter and to CO adsorption on the interface sites, where such effects can be substantial.
- For adsorption on top layer sites, these latter effects are negligible, except for coordination effects, and adsorption resembles that on metal surfaces. For adsorption on interface sites, these effects can be substantial, depending on the position of the O-vacancy. The systematic difference in CO adsorption energy between interface (i) and interface (ii) sites is mainly due to higher positive contributions from CO_{ad} induced deformation energies and changes in interface energy. For adsorption on the middle layer Ru-5a site, its higher adsorption energy is mainly attributed to coordination effects. Contributions from charge transfer to the Ru adsorption site, or deformation/interface energies are generally small, and except for a single case direct interactions between CO and a partly reduced Zr surface ion do not play an important role.

- The vibrational properties of the CO molecules generally follow the trend of the adsorption energies and of the charge transfer from the Ru nanorod to the CO molecules upon adsorption, except for the adsorption at the interface sites, where they can be modified significantly by interaction with the ZrO_2 support.
- Adsorbed CO will generally lead to a stabilization of O-vacancies and therefore to a lower O-vacancy formation energy.

In combination, these results provide a detailed picture of the formation and stability of O-vacancies in ZrO_2 in the presence of a Ru nanoparticle, of the related charge transfer from the ZrO_2 support to the Ru nanorod, and of the impact of O-vacancies on the CO adsorption properties, including trends in the CO adsorption energies on different Ru sites, on CO adsorption induced charge transfer, and in the C-O vibrational frequencies. They indicate a wide variation of the CO adsorption energies and vibrational frequencies on different sites, which under equilibrium conditions will be populated according to their stability. While the numbers are specific for the present system, the general effects and the contributions for adsorption on interface sides, higher layer sites and the transition layer directly on top of the interface metal layer are considered to be of general validity. In this sense, they are of general relevance for the understanding of electronic metal-support interactions (EMSIs) and their impact on adsorption and catalytic reactions on catalyst systems consisting of metal nanoparticles supported on reducible oxides.

ASSOCIATED CONTENT

Supporting Information

The Supporting Information is available free of charge at https://pubs.acs.org/doi/10.1021/acscatal.xxxxxxx.

Table S1-S5: O-vacancy formation energies; Figure S1: Schematic representation of the different contributions to the energy required for the formation of O-vacancies; Table S6 – S21: CO adsorption configurations; Table S22 – S29: CO adsorption energies; Figure S2: Schematic representation of the different contributions to the CO adsorption energy on a Ru/ZrO_{2-x} model system; Table S30 – S33: Charge distribution in model systems with O-vacancies underneath the Ru nanorod; Table S34 – S40: Charge distribution in model systems with O-vacancies aside the Ru nanorod; Table S41 – S46: Charge distribution in model systems with O-vacancies in deeper layers underneath the Ru nanorod; Table S47 – S56: Energies of the center of the d-band for model systems with O-vacancies underneath the Ru nanorod

AUTOR INFORMATION

Corresponding Author

R. Jürgen Behm − Institute of Theoretical Chemistry, Ulm University, D-89081 Ulm, Germany; orcid.org/0000-0002-7565-0628; Email: juergen.behm@uni-ulm.de

Authors

Mengru Li − Institute of Theoretical Chemistry, Ulm University, D-89081 Ulm, Germany

Axel Groß − Institute of Theoretical Chemistry, Ulm University, D-89081 Ulm, Germany; orcid.org/0000-0003-4037-7331

Notes

The authors declare no competing financial interest

Acknowledgements

Computer time provided by the state of Baden-Württemberg through the bwHPC project and by the DFG under Grant No. INST 40/575-1 FUGG (JUSTUS 2 cluster) is gratefully acknowledged.

References

1. Che, M.; Bennet, C. O. The Influence of Particle Size on the Catalytic Properties of Supported Metals, *Adv. Catal.* **1989**, *36*, 55-172.
2. Bell, A. T. The Impact of Nanoscience on Heterogeneous Catalysis, *Science* **2003**, *299*, 1688-1691.
3. Ertl, G.; Knözinger, H.; Schüth, F.; Weitkamp, J. *Handbook of Heterogeneous Catalysis - Table of Contents*, 2 ed.; VCH-Wiley: Weinheim, 2008.
4. van Deelen, T. W.; Hernandez Mejia, C.; de Jong, K. P. Control of Metal-Support Interactions in Heterogeneous Catalysts to Enhance Activity and Selectivity, *Nat. Catal.* **2019**, *2*, 955-970.
5. Tauster, S. J.; Fung, S. C.; Garten, R. L. Strong Metal-Support Interactions. Group 8 Noble Metals Supported on TiO_2, *J. Am. Chem. Soc.* **1978**, *100*, 170-175.
6. Tauster, S. J.; Fung, S. C.; Baker, R. T. K.; Horsley, J. A. Strong Interactions in Supported-Metal Catalysts, *Science* **1981**, *211*, 1121-1125.
7. Haller, G. L.; Resaco, D. E. Metal-Support Interaction: Group VIII Metals and Reducible Oxides, *Adv. Catal.* **1989**, *36*, 173-234.
8. Campbell, C. T. Catalyst-Support Interactions: Electronic Perturbations, *Nat. Chem.* **2012**, *4*, 597-598.
9. Bruix, A.; Rodriguez, J. A.; Ramírez, P. J.; Senanayake, S. D.; Evans, J.; Park, J. B.; Stacchiola, D.; Liu, P.; Hrbek, J.; Illas, F. A New Type of Strong Metal-Aupport Interaction and the Production of H_2 Through the Transformation of Water on $Pt/CeO_2(111)$ and $Pt/CeO_x/TiO_2(110)$ Catalysts, *J. Am. Chem. Soc.* **2012**, *134*, 8968-8974.
10. Ruiz Puigdollers, A.; Schlexer, P.; Tosoni, S.; Pacchioni, G. Increasing Oxide Reducibility: The Role of Metal/Oxide Interfaces in the Formation of Oxygen Vacancies, *ACS Catal.* **2017**, *7*, 6493-6513.
11. Pacchioni, G.; Freund, H. J. Controlling the Charge State of Supported Nanoparticles in Catalysis: Lessons From Model Systems, *Chem. Soc. Rev.* **2018**, *47*, 8474-8502.
12. Wang, W.; Zhang, X.; Weng, S.; Peng, C. Tuning Catalytic Activity of CO_2 Hydrogenation to C1 Product Via Metal Support Interaction Over Metal/Metal Oxide Supported Catalysts, *ChemSusChem* **2024**, *n/a*, e202400104.
13. Campbell, C. T.; Sellers, J. R. V. Anchored Metal Nanoparticles: Effects of Support and Size on Their Energy, Sintering Resistance and Reactivity, *Faraday Discuss.* **2013**, *162*, 9-30.

14. Hemmingson, S. L.; Campbell, C. T. Trends in Adhesion Energies of Metal Nanoparticles on Oxide Surfaces: Understanding Support Effects in Catalysis and Nanotechnology, *ACS Nano* **2017**, *11*, 1196-1203.

15. Schubert, M. M.; Hackenberg, S.; van Veen, A. C.; Muhler, M.; Plzak, V.; Behm, R. J. CO Oxidation Over Supported Gold Catalysts - 'Inert' and 'Active' Support Materials and Their Role for the Oxygen Supply During Reaction, *J. Catal.* **2001**, *197*, 113.

16. Schlexer, P.; Widmann, D.; Behm, R. J.; Pacchioni, G. CO Oxidation on a Au/TiO_2 Nanoparticle Catalyst Via the Au-Assisted Mars-Van-Krevelen Mechanism, *ACS Catal.* **2018**, *8*, 6513-6525.

17. Schlexer, P.; Ruiz Puigdollers, A.; Pacchioni, G. Role of Metal/Oxide Interfaces in Enhancing the Local Oxide Reducibility, *Top. Catal.* **2018**, *61*, 1-10.

18. Widmann, D.; Behm, R. J. Active Oxygen on a Au/TiO_2 Catalyst - Formation, Stability and CO Oxidation Activity, *Angew. Chem. Int. Ed.* **2011**, *50*, 10241-10245.

19. Widmann, D.; Behm, R. J. Activation of Molecular Oxygen and the Nature of the Active Oxygen Species for CO Oxidation on Oxide Supported Au Catalysts, *Acc. Chem. Res.* **2014**, *47*, 740-749.

20. Chen, S.; Abdel-Mageed, A. M.; Li, M.; Cisneros, S.; Bansmann, J.; Rabeah, J.; Brückner, A.; Groß, A.; Behm, R. J. Electronic Metal-Support Interactions and Their Promotional Effect on CO_2 Methanation on Ru/ZrO_2 Catalysts, *J. Catal.* **2021**, *400*, 407-420.

21. Li, M.; Gross, A.; Behm, R. J. Effect of O-Vacancy Concentration and Proximity on Electronic Metal-Support Interactions: Ru/ZrO_2 Catalysts, *ACS Catal.* **2022**, *12*, 10065-10079.

22. Ni, J.; Leng, W.; Mao, J.; Wang, J.; Lin, J.; Jiang, D.; Li, X. Tuning Electron Density of Metal Nickel by Support Defects in Ni/ZrO_2 for Selective Hydrogenation of Fatty Acids to Alkanes and Alcohols, *Appl. Catal. B* **2019**, *253*, 170-178.

23. Chakarova, K.; Mihaylov, M.; Ivanova, S.; Centeno, M. A.; Hadjiivanov, K. Well-Defined Negatively Charged Gold Carbonyls on Au/SiO_2, *J. Phys. Chem. C* **2011**, *115*, 21273-21282.

24. Meunier, F. C.; Wang, X.; Bürgi, T. On the Reality of Negatively Charged Supported Gold Nanoparticles, *J. Catal.* **2023**, *425*, 345-349.

25. Sabatier, P. Hydrogénations Et Déshydrogénations Par Catalyse, *Ber. Dtsch. Chem. Ges.* **1911**, *44*, 1984-2001.

26. Ahmadi, M.; Mistry, H.; Roldan Cuenya, B. Tailoring the Catalytic Properties of Metal Nanoparticles Via Support Interactions, *J. Phys. Chem. Lett.* **2016**, *7*, 3519-3533.

27. Kresse, G.; Hafner, J. Ab Initio Molecular-Dynamics Simulation of the Liquid Metal–Amorphous-Semiconductor Transition in Germanium, *Phys. Rev. B* **1994**, *49*, 14251-14269.

28. Kresse, G.; Furthmüller, J. Efficiency of Ab-Initio Total Energy Calculations for Metals and Semiconductors Using a Plane-Wave Basis Set, *Comp. Mat. Sci.* **1996**, *6*, 15-50.

29. Kresse, G.; Furthmüller, J. Efficient Iterative Schemes for Ab Initio Total-Energy Calculations Using a Plane-Wave Basis Set, *Phys. Rev. B* **1996**, *54*, 11169-11186.

30. Blöchl, P. E. Projector Augmented-Wave Method, *Phys. Rev. B* **1994**, *50*, 17953-17979.

31. Kresse, G.; Joubert, D. From Ultrasoft Pseudopotentials to the Projector Augmented-Wave Method, *Phys. Rev. B* **1999**, *59*, 1758-1775.

32. Perdew, J. P.; Burke, K.; Ernzerhof, M. Generalized Gradient Approximation Made Simple, *Phys. Rev. Lett.* **1996**, *77*, 3865-3868.

33. Dudarev, S. L.; Botton, G. A.; Savrasov, S. Y.; Humphreys, C. J.; sutton, A. P. Electron-Energy-Loss Spectra and the Structural Stability of Nickel Oxide: An LSDA+U Study, *Phys. Rev. B* **1998**, *57*, 1505-1509.

34. Wang, L.; Maxisch, T.; Ceder, G. Oxidation Energies of Transition Metal Oxides Within the GGA+U Framework, *Phys. Rev. B* **2006**, *73*, 195107.

35. Tolba, S. A.; Allam, N. K. Computational Design of Novel Hydrogen-Doped, Oxygen-Deficient Monoclinic Zirconia With Excellent Optical Absorption and Electronic Properties, *Sci. Rep.* **2019**, *9*, 10159.

36. Grimme, S.; Ehrlich, S.; Goerigk, L. Effect of the Damping Function in Dispersion Corrected Density Functional Theory, *J. Comput. Chem.* **2011**, *32*, 1456-1465.

37. Monkhorst, H. J.; Pack, J. D. Special Points for Brillouin-Zone Integrations, *Phys. Rev. B* **1976**, *13*, 5188-5192.

38. Manz, T. A.; Limas, N. G. Introducing DDEC6 Atomic Population Analysis: Part 1. Charge Partitioning Theory and Methodology, *RSC Adv.* **2016**, *6*, 47771-47801.

39. Limas, N. G.; Manz, T. A. Introducing DDEC6 Atomic Population Analysis: Part 2. Computed Results for a Wide Range of Periodic and Nonperiodic Materials, *RSC Adv.* **2016**, *6*, 45727-45747.

40. Sakong, S.; Groß, A. The Electric Double Layer at Metal-Water Interfaces Revisited Based on a Charge Polarization Scheme, *J. Chem. Phys.* **2018**, *149*, 084705.

41. Hammer, B.; Nørskov, J. K. Theoretical Surface Science and Catalysis-Calculations and Concepts, *Adv. Catal.* **2000**, *45*, 71-129.

42. Blyholder, G. Molecular Orbital View of Chemisorbed Carbon Monoxide, *J. Phys. Chem.* **1964**, *68*, 2772-2778.

43. Hammer, B.; Nielsen, O. H.; Nørskov, J. K. Structure Sensitivity in Adsorption: CO Interaction With Stepped and Reconstructed Pt Surfaces, *Catal. Lett.* **1997**, *46*, 31-35.

44. Calle-Vallejo, F.; Martinez, J. I.; Garcia-Lastra, J. M.; Sautet, P.; Loffreda, D. Fast Prediction of Adsorption Properties for Platinum Nanocatalysts With Generalized Coordination Numbers, *Angew. Chem. Int. Ed.* **2014**, *53*, 8316-8319.

45. Hammer, B.; Nørskov, J. K. Electronic Factors Determining the Reactivity of Metal Surfaces, *Surf. Sci.* **1995**, *343*, 211-220.

46. Mavrikakis, M.; Hammer, B.; Nørskov, J. K. Effect of Strain on the Reactivity of Metal Surfaces, *Phys. Rev. Lett.* **1998**, *81*, 2819-2822.